LncRNA *TAAL* is a Modulator of *Tie1*-Mediated Vascular Function in Diabetic Retinopathy

Gyan Ranjan[1,2 *], Samriddhi Arora[1], Sarmeela Sharma[3], Lakshita Sharma[2], Rahul C Bhoyar[2], Vigneshwar Senthivel[2], Vinod Scaria[2, 4, 5], Subhabrata Chakrabarti[3], Inderjeet Kaur[3], Sridhar Sivasubbu[2, 4, 5 *], Rajender K Motiani[1,*]

[1] Laboratory of Calciomics and Systemic Pathophysiology, Regional Center for Biotechnology (RCB), Faridabad, India.
[2] CSIR Institute of Genomics and Integrative Biology, New Delhi, India.
[3] Brien Holden Eye Research Centre L V Prasad Eye Institute Hyderabad, India.
[4] Vishwanath Cancer Care Foundation, Mumbai, India.
[5] Dr. D. Y Patil Medical College, Hospital and Research Centre, Pune, India.

*Corresponding authors:-

Dr. Gyan Ranjan
Postdoctoral Research Associate - Regional Centre for Biotechnology (RCB)
Faridabad, Delhi-NCR, India
Email: gyanranjan2197@gmail.com; gyan.ranjan@rcb.res.in

Dr. Rajender K Motiani
Associate Professor - Regional Centre for Biotechnology (RCB)
Faridabad, Delhi-NCR, India
Email: rajender.motiani@rcb.res.in

Dr. Sridhar Sivasubbu
Chief Scientist, CSIR Institute of Genomics and Integrative Biology (CSIR-IGIB),
New Delhi, India
Present address:
Senior Consultant, Vishwanath Cancer Care Foundation, Mumbai, India
Adjunct Professor, Dr. D. Y Patil Medical College, Hospital and Research Centre, Pune, India
Email: sridhar@igib.in ; sridhar.sivasubbu@gmail.com

Abstract.

Diabetic retinopathy (DR), a leading cause of vision impairment and blindness, is characterized by abnormal retinal vascular changes due to chronic hyperglycemia. The *Tie-1* signaling pathway, essential for vascular growth and remodeling, has emerged as a key therapeutic target, though its molecular mechanisms and interactome remain largely unclear. Through a protein-centric approach, we identified a novel lncRNA and named it *Tie1-associated angiogenic lncRNA (TAAL)*. *TAAL* lncRNA regulates endothelial cell migration, proliferation, tube formation, and permeability by modulating ER-calcium homeostasis and cytoskeleton dynamics. In zebrafish, *taal* modulation led to angiogenic defects, which were rescued by human *TAAL* orthologue. Our molecular studies further revealed that *TAAL* negatively regulates *Tie1* protein via ubiquitin-mediated degradation. Notably, *TAAL* expression is upregulated in the blood of DR patients and downregulated in endothelial DR cell models. Overexpression of *TAAL* restored endothelial permeability and VE-cadherin surface expression. These findings establish *TAAL* as a novel regulator of *Tie1* protein turnover, with potential therapeutic implications for diabetic retinopathy.

Keywords

lncRNA, Diabetic Retinopathy, *Tie1*, endothelial, zebrafish, permeability, vascular

Synopsis

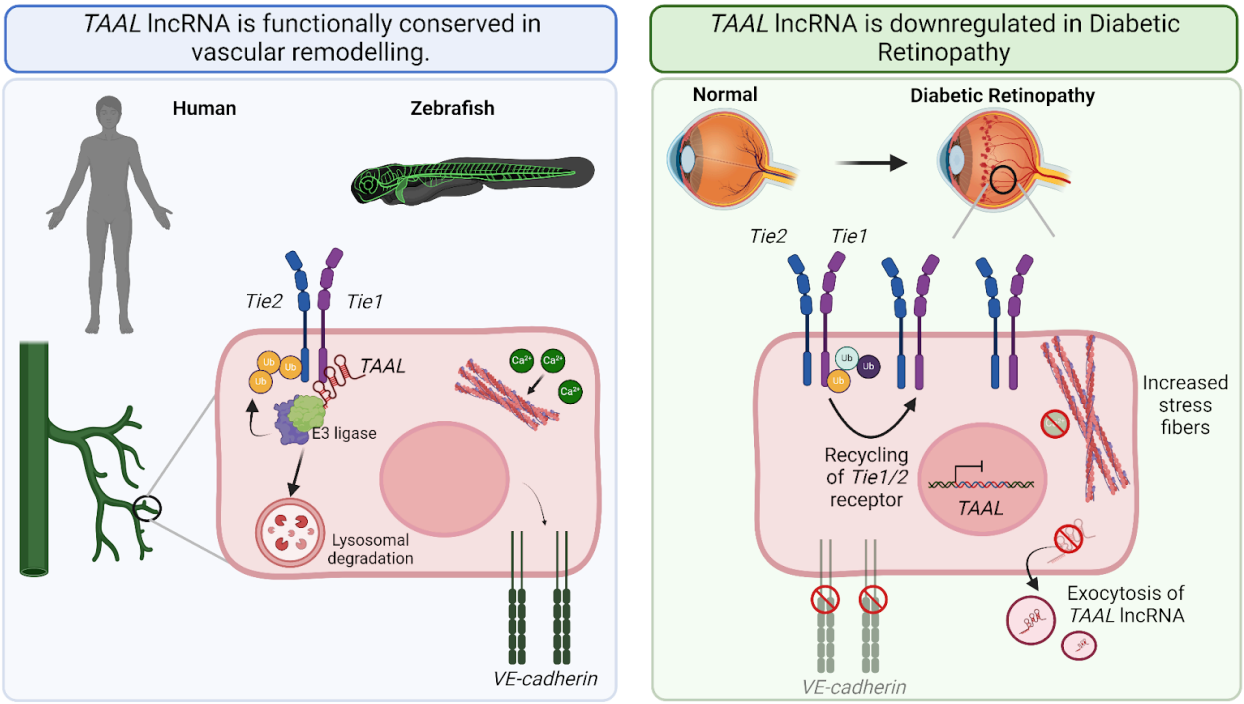

Tie1 is an endothelial protein that plays a critical role in neovascularization. Its interactome is not well studied. Here, we discover a novel lncRNA *TAAL* that interacts with *Tie1* protein and regulates its protein turnover thereby, *TAAL* modulates endothelial pathophysiology.

- The *TAAL* lncRNA interacts with the *Tie1* protein and regulates vascular remodeling.
- The *TAAL* lncRNA is functionally conserved between human and zebrafish. It plays an important role in regulating vascular angiogenesis during development.
- The *TAAL* lncRNA controls the protein turnover of *Tie1* by ubiquitin-mediated modulation of its stabilization and translation.
- The *TAAL* lncRNA is hyperactive during diabetic retinopathy and is a potential biomarker and a potent therapeutic target.

Introduction

Diabetes mellitus (DM) is a chronic metabolic disorder characterized by persistent hyperglycemia, which can have detrimental effects on multiple organs, including the kidneys, liver, and cardiovascular system. Among the most serious complications of DM is diabetic retinopathy (DR), a condition driven by abnormal retinal neovascularization and dysregulated angiogenesis. These pathological changes increase vascular permeability, leading to retinal hemorrhage and, in severe cases, vision impairment or blindness (Wong *et al*, 2016; Duh *et al*, 2017). It is estimated that approximately 1 in 5 individuals with diabetes develop some degree of DR, with the incidence being particularly high in low- and middle-income countries where late diagnosis is common due to resource constraints. Early detection of DR is crucial, as timely intervention can prevent up to 95% of vision impairment and blindness. Current treatment strategies include laser therapy, vitrectomy, and anti-VEGF therapies (Wong *et al*, 2016; Duh *et al*, 2017). However, the prevalence of DR is rising rapidly, and there remains a significant unmet need for cost-effective, point-of-care diagnostic tools and targeted second-generation therapies to manage better and control the progression of this condition. Recent studies have shown that angiopoietin and *Tie* signaling plays a crucial role in protecting vascular dysfunction. During hyperglycemic conditions, the Ang-Tie signaling is severely affected (Saharinen *et al*, 2017).

Tie1 is a major effector protein during hyperglycemic conditions as it is a major player in neovascularization. Although its interactome and ligand remain a mystery, and it is often termed an orphan receptor (Mueller & Kontos, 2016; Sato *et al*, 1995). Recent investigations have shed light on their more complex involvement in regulating endothelial homeostasis and remodeling. *Tie1* in zebrafish and mice has been shown to affect endothelial cell angiogenesis and proper homeostasis *in vivo* (Carlantoni *et al*, 2021; Reinardy *et al*, 2015; D'Amico *et al*, 2010).

Moreover, functional studies indicate that *Tie1* plays a dual role in angiogenesis: it exerts a negative regulatory effect on *Tie2* levels within angiogenic tip cells, while positively regulating *Tie2* by forming heterodimers in stalk cells (Savant *et al*, 2015). These heterodimers are crucial for the maturation and remodeling of vessels through angiopoietin 1 signaling. Previous investigations suggested that Angiopoietin-1 binding independently to Tie2 and in heterodimeric association with *Tie1*, activating downstream signaling kinases such as PI3K/Akt pathway or Rho/Rac1, thereby modulating endothelial cell proliferation, migration, and survival(Saharinen *et al*, 2017; Joussen *et al*, 2021; Papapetropoulos *et al*, 2000; Saharinen *et al*, 2008). The regulation of *Tie1* and *Tie2* levels in vascular remodeling has been a focal point of research due to their potential as targeted therapies. Their involvement in diseases such as cancer metastasis and diabetic retinopathy underscores their clinical significance (Saharinen *et al*, 2017; Huang *et al*, 2010; Joussen *et al*, 2021; Augustin *et al*, 2009). It has prompted intensive investigation as they are the key player in angiogenesis and endothelial function.

Long noncoding RNAs (lncRNAs) are a significant and abundant class of regulatory molecules in endothelial cells, where they play a crucial role in controlling gene expression at various levels, including chromatin remodeling, transcription, and post-transcriptional processing. Recent discoveries, such as lncRNAs like *VEAL2, GATA-AS, SENCR, LASSI, STEEL, MANTIS, LEENE,* and *Tie1-AS*, have underscored their essential functions in regulating endothelial cell proliferation, migration, permeability, and stability. These lncRNAs have been extensively studied, revealing new mechanisms of action and interactions that continue to emerge. In addition to their regulatory roles, lncRNAs have shown promise as biomarkers for vascular diseases, given their high specificity, offering potential for early diagnosis and personalized treatment strategies. Given their pivotal role in vascular biology, lncRNAs are

122 increasingly recognized as both therapeutic targets and biomarkers for managing conditions like
123 diabetic retinopathy, where novel RNA-based interventions could provide significant clinical
124 benefits.

125 This study explores the RNA interactions of *Tie1*, a key protein involved in
126 neovascularization and complications in diabetic retinopathy (DR). Through a Tie1 pulldown
127 approach, we identified a previously uncharacterized and conserved lncRNA, *TAAL*, in human
128 endothelial cells and zebrafish. Our research highlights the critical role of lncRNA *TAAL* in
129 fundamental physiological processes such as tube formation and vascular permeability in
130 endothelial cells, with significant implications for vascular development in zebrafish embryos.
131 Notably, we discovered a crucial interaction between lncRNA *TAAL* and the *Tie1* protein, where
132 *TAAL* is essential for modulating *Tie1* protein stability. This relationship was further examined in
133 the context of DR, where lncRNA *TAAL* levels were notably upregulated in patient samples
134 compared to controls. These findings emphasize the importance of lncRNA *TAAL* in regulating
135 *Tie1*-mediated angiogenesis, permeability and vascular functions, particularly under diabetic
136 retinopathy conditions.

137 **Results**

138 **Protein-centric discovery of novel lncRNA - *Tie1*-associated angiogenic lncRNA**
139 **(*TAAL*)**

140 *Tie-1* plays a critical role in vascular development, as demonstrated in the mouse and zebrafish
141 models(Cao *et al*, 2023; Savant *et al*, 2015; Carlantoni *et al*, 2021). However, *Tie-1*'s interactome
142 and the molecular mechanisms regulating its expression remain poorly understood. Here, we
143 performed a protein-targeted pulldown of *Tie1* and determined if any *Tie1* protein-associated
144 long non-coding RNAs are involved in the angiogenesis pathway using HUVEC-hTert2 cell line.

145 We performed RNA immunoprecipitation (RIP) of *Tie1* protein followed by RNA-sequencing
146 (Figure 1A). After applying a stringent cutoff filter of greater than 5 fold change and -$\log_{10}$
147 (P-value) value greater than 2, we identified a bi-exonic polyadenylated lncRNA (Supply Fig
148 1A) and named it *TIE1-associated angiogenic lncRNA (TAAL) (previous names-*
149 *ENST00000457948.3, NONHSAG007003.2, RP11-79M19.2)(*Figure 1B). The lncRNA originates
150 from the intron between 2 and 3 exons of the GRK5 gene (Figure 1C). Further, it does not
151 exhibit any coding potential as computed using bioinformatic algorithms (Coding Potential
152 Assessment Tool (CPAT2) coding probability - 0.0003 (Wang *et al*, 2013); Coding Potential
153 Calculator (CPC2) coding probability - 0.0216282 (Kang *et al*, 2017))(Supply Fig 1B) . We also
154 performed ribosomal pulldown followed by RT-qPCR of the *TAAL* lncRNA and did not find any
155 ribosome enrichment on lncRNA *TAAL*, further suggesting it to be non-coding (Supply Fig 1C).
156 The second exon and promoter of lncRNA *TAAL* is observed to be conserved in mammals and
157 birds but is lost in reptiles and fish, exhibiting no sequence conservation. It also displays all the
158 epigenomic marks, including H3K27ac, H3K4me1, H3K4me3, and CAGE reads from ENCODE
159 data in HUVECs, suggesting it is a genuine transcript (Figure 1C) (ENCODE Project
160 Consortium *et al*, 2020). Expression profiling of the lncRNA using the GTEx v8 portal exhibited
161 it highly expressed in the testis, ovary, pituitary, lungs, and heart tissues (Supply Fig 2A)(Ferraro
162 *et al*, 2020). Next, we performed RIP-RT-qPCR to determine if the *TAAL* lncRNA also interacts
163 with *Tie2*. We did not find any enrichment of the lncRNA to the *Tie2* protein (Figure 1D).
164 Furthermore, to understand its localization, we performed subcellular fractionation and
165 qRT-PCR, which suggested that the *TAAL* lncRNA is cytoplasmic enriched (Figure 1E).
166 Single-molecule RNA *FISH* (*smFISH*) also demonstrates that *TAAL* lncRNA is enriched in the
167 cytoplasm (Supply Fig2B). We also performed co-immunofluorescent and *smFISH* for *TAAL*

168 lncRNA, *Tie1*, and *Tie2* proteins and observed colocalization of the lncRNA and proteins (Figure
169 1F). The interaction of *TAAL* lncRNA along with the *Tie1* protein suggests its *trans*-role in
170 regulating protein function.
171
172 **LncRNA *TAAL* modulates the pathophysiological functions of endothelial cells.**
173 To understand the functionality of the lncRNA, we performed siRNA-mediated knockdown
174 using siTAAL and overexpression using pcDNA3.1-TAAL plasmid. We observed significant
175 knockdown and overexpression of the *TAAL* lncRNA transcript *in vivo* in the HUVEC-hTert2
176 cell line (Supply Fig 3 A-B). Next, we conducted scratch-wound assays and transwell migration
177 assays to elucidate the migratory properties of cells upon lncRNA *TAAL* manipulation.
178 Remarkably, the knockdown of lncRNA *TAAL* promoted enhanced wound closure and increased
179 the migratory capacity of cells. In contrast, overexpression of lncRNA *TAAL* exerted a decrease
180 in wound closure rate and an inhibitory effect on cell migration (Figure 2A-D). Additionally,
181 BrdU proliferation assays corroborated our findings, demonstrating increased cell proliferation
182 following lncRNA *TAAL* knockdown, while overexpression of lncRNA *TAAL* attenuated cellular
183 proliferation (Figure 2E-F). Moreover, cell cycle analysis unveiled distinct alterations in cell
184 cycle distribution patterns associated with lncRNA *TAAL* modulation. Specifically, the
185 knockdown of lncRNA TAAL led to an accumulation of cells in the G0/G1 phase, indicative of
186 an active proliferative state. In contrast, overexpression of lncRNA TAAL showed no significant
187 change (Supply Fig I-J). Furthermore, we conducted a permeability assay using a
188 collagen-coated transwell plate to assess the impact of lncRNA *TAAL* on cellular permeability.
189 We observed a significant increase in permeability following the knockdown of lncRNA *TAAL*

190 (Figure 2G). Conversely, we noted a decrease in permeability upon the overexpression of
191 lncRNA *TAAL*, suggesting lncRNA's role in maintaining cellular barrier integrity (Figure 2H).
192 Next, we evaluated the angiogenic tube-forming function of the HUVEC-hTert2 cell under
193 knockdown and overexpression conditions. We observed that lncRNA *TAAL* knockdown cells
194 *(siTAAL)* were forming colonies but could not attain the tubular morphology on matrigel
195 compared to control transfection *(siControl)*. Similarly, upon *TAAL* lncRNA overexpression
196 (*pcDNA-TAAL*), we observed that cells could not attain the tubular morphology as seen in the
197 control pcDNA-3.1 transfection condition (Figure 2I-J). Next, we investigated cell viability's
198 potential influence on the perturbations in tubulogenesis observed upon manipulating lncRNA
199 *TAAL* expression levels. To comprehensively assess cell viability, we performed Annexin-V/PI
200 staining assays. We observed no significant change in cell viability following transfection with
201 siTAAL and pcDNA-*TAAL* constructs, suggesting the effects are not due to cellular toxicity but
202 rather the modulation of lncRNA *TAAL* expression (Figure 2K-L). These data together suggest
203 that lncRNA *TAAL* modulates the physiological function of endothelial cells.
204

205 **LncRNA *TAAL* regulates calcium-dependent cytoskeletal and junctional**
206 **dynamics.**

207 Given the observed alterations in proliferation and migration, we investigated the impact of
208 lncRNA *TAAL* modulation on cellular cytoskeletal dynamics. In the endothelial cells, we stained
209 the F-actin using Alexa Fluor 488 phalloidin to visualize cytoskeletal structures. Our analysis
210 revealed noteworthy changes in cytoskeletal organization upon knockdown and overexpression
211 of *TAAL* lncRNA. Specifically, *TAAL* lncRNA knockdown cells exhibited a marked increase in
212 the length and density of stress fibers, indicative of enhanced cytoskeletal stiffness (Figure 3A).

213 Furthermore, these cells elongated in cell length compared to their respective controls (Supply
214 Fig 5A). Conversely, overexpression of *TAAL* lncRNA elicited contrasting effects, with cells
215 displaying a reduction in both stress fiber length and cell size (Figure 3A). This suggests a role
216 for *TAAL* lncRNA in modulating cytoskeletal dynamics and cellular stiffness, potentially
217 influencing cellular morphology and migration ability.

218 Previous investigations have highlighted the involvement of endoplasmic reticulum (ER)
219 calcium dynamics in mediating cytoskeletal remodeling in endothelial cells (Shinde *et al*, 2013;
220 Tsai & Meyer, 2012; Tsai *et al*, 2014). Angiopoietin 1/2 mediated calcium regulation via the *Tie*
221 receptors has also been previously investigated and has been linked to angiogenesis (Pafumi *et*
222 *al*, 2015). Hence we investigated the impact of lncRNA *TAAL* modulation on intracellular
223 calcium levels, specifically focusing on calcium regulation within the ER. We assessed changes
224 in calcium dynamics by using live cell Ca^{2+} imaging with the ratiometric dye Fura2-AM.
225 Additionally, we employed the pharmacological inhibitor Thapsigargin (Tg) to deplete ER Ca^{2+}
226 stores, aiming to elucidate the role of *TAAL* in calcium homeostasis. Our observations revealed
227 significant alterations in calcium homeostasis upon manipulating lncRNA *TAAL* expression
228 levels. The knockdown of lncRNA *TAAL* resulted in a significant decrease in basal intracellular
229 calcium levels and a reduction in ER calcium content (Figure 3B-D). Conversely, overexpression
230 of lncRNA *TAAL* led to increased basal intracellular calcium levels and ER calcium content
231 (Figure 3E-G). Consistent with previous findings in cell culture and zebrafish models, which
232 have demonstrated that calcium spikes induce stress fiber contraction (Stolz & Bereiter-Hahn,
233 1988; Tiruppathi *et al*, 2002; Shinde *et al*, 2013; Dalal *et al*, 2020; Sahu *et al*, 2017), our results
234 suggest that changes in cytoskeletal dynamics associated with lncRNA *TAAL* modulation may be
235 mediated through alterations in calcium influx. We also checked the expression levels of a few

236 calcium modulator genes and observed that STIM1 levels were downregulated in *TAAL*
237 overexpressed cells (Supply Fig 6A-B). Also, upon modulation of lncRNA *TAAL*, the levels of
238 *STIM2* were significantly altered; in the knockdown state, it was suppressed, and in
239 overexpression of lncRNA, it was upregulated, correlating with the calcium levels inside the cell
240 upon similar conditions (Supply Fig 6C-D). We also observed decreased ORAI2 leaves upon
241 *TAAL* overexpression in the cells (Supply Fig 6 E-F). This suggests that intracellular calcium
242 dynamics, upon modulation of lncRNA *TAAL*, are governed by alterations in the levels of *STIM*
243 proteins,, a critical regulator of cellular and ER calcium homeostasis.

244 To further elucidate the underlying mechanisms contributing to changes in cellular
245 permeability following lncRNA *TAAL* alteration, we assessed mRNA levels of *VEGFR2* (KDR)
246 and VE-Cadherin (Hamdollah Zadeh *et al*, 2008; Phoenix *et al*, 2022; Bates & Curry, 1997;
247 Dalal *et al*, 2020; Gavard, 2013; Sandoval *et al*, 2001) but observed no significant changes
248 (Supplementary Fig 7A-D) . Next, we examined the localization of VE-Cadherin, an adhesion
249 protein regulated by the *Tie1-Tie2* signaling pathway and calcium influx. Our analysis revealed
250 that *TAAL* knockdown resulted in decreased membrane localization of VE-Cadherin, while *TAAL*
251 overexpression increased its membrane localization (Figure 3H). These findings collectively
252 suggest that modulation of lncRNA *TAAL* influences the VE-Cadherin membrane localization.

253

254 **_TAAL_ lncRNA is functionally conserved in zebrafish and modulates angiogenesis.**

255 To check if the lncRNA is functionally conserved across species, we performed a protein-centric
256 pulldown of *tie1* in zebrafish at 24 hpf, followed by RNA sequencing. Upon analysis, we
257 observed a lncRNA *ZFLNCG09997* (hereafter called lncRNA *taal*) was 4.7 fold enriched and
258 had a $-\log_{10}$ P-value greater than 15 (Figure 4A-B). The zebrafish *taal* lncRNA gene produces a 3

exonic polyadenylated lncRNA (Supply Fig 8A) with a transcript length of 2632bp observed on chromosome 18 of zebrafish, arises antisense 5' upstream of endonuclease, polyU-specific C (*endouc*). The *taal* lncRNA is noncoding in nature, as assessed through the online tool Coding Potential Calculator (CPC2) (coding probability -0.0403034), and has no potential predicted ORF. The *taal* lncRNA shows no sequence conservation with its human orthologue *TAAL*.

The expression profile analysis across adult tissues and developmental stages using publicly available RNA seq data (Pauli *et al*, 2012; Yang *et al*, 2020; Sehgal *et al*, 2021) unveiled the expression of the lncRNA in zebrafish's heart, testis, and skin (Figure 4C). We also observed a prominent expression peak of the lncRNA *taal* during the bud stage, followed by sustained expression at 48 hours post-fertilization (hpf) and 5 days post-fertilization (dpf) (Figure 4D). Intriguingly, an inverse expression pattern was observed for the protein-coding genes *tie1* and *tie2* at 24 hpf, where their expression levels were markedly elevated while lncRNA *taal* expression remained minimal. Notably, the initiation of angiogenesis from the posterior cardinal vein (PCV) occurs during this developmental stage, implicating *tie1* and *tie2* in the sprouting and angiogenesis process. The observed expression pattern of lncRNA *taal* suggests a potential inhibitory role for *tie1* and *tie2* in angiogenesis during this critical developmental stage.

An antisense splice-blocking morpholino-based knockdown approach was employed to elucidate further the functional significance of lncRNA *taal* in zebrafish development. Knockdown of lncRNA *taal* resulted in notable defects in zebrafish angiogenesis, particularly evident in patterning defects observed in the intersegmental vessels (ISVs) at 2 dpf (Figure 4E). Additionally, investigation into the role of lncRNA *taal* in angiogenesis revealed enhanced angiogenic sprouting from the subintestinal vessels (SIVs) in zebrafish injected with taal morpholino near the SIV site as compared to control injections with scramble morpholino,

282 indicative of an anti-angiogenic role for lncRNA *taal*. Further confirmation of lncRNA *taal's*
283 functional conservation across species was attained through complementation and rescue assays.
284 Injection of a wild-type copy of human lncRNA *TAAL* demonstrated a reduction in angiogenic
285 sprouting when co-injected with *taal* morpholino, affirming the orthologous nature of lncRNA
286 *taal* between humans and zebrafish (Figure 4F). Moreover, an overexpression experiment of
287 lncRNA *TAAL* injected into the single-cell zebrafish embryos revealed abnormal vascular
288 patterning (Figure 4G). Furthermore, the injection of *TAAL* lncRNA at the SIV site led to a
289 reduction in the area of the SIV vessel formation (Figure H). This suggests a pivotal role of
290 zebrafish *taal* lncRNA in modulating angiogenic processes. These findings provide compelling
291 evidence that zebrafish *taal* lncRNA is a functional orthologue to human *TAAL* lncRNA and has
292 an important role in modulating and controlling angiogenic function in vertebrates.
293

294 **LncRNA *TAAL* negatively regulates *Tie1/2* protein turnover.**

295 To understand the molecular mechanism we examined the expression pattern of *Tie1* and *Tie2*
296 protein, with which the lncRNA *TAAL* interacts. We observed an increase in the protein
297 expression upon knockdown of the lncRNA *TAAL* and a decrease in the expression upon
298 overexpression of the lncRNA (Figure 5A). We also estimated *Tie1* and *Tie2* mRNA levels and
299 found no significant change in their mRNA expression upon knockdown and overexpression of
300 the lncRNA *TAAL* (Figure 5B). These findings indicate that lncRNA *TAAL* post-translationally
301 regulates the levels of *Tie1* and *Tie2* in endothelial cells. To further investigate this regulation, we
302 conducted immunofluorescence analysis of *Tie1* and *Tie2* under lncRNA *TAAL* knockdown and
303 overexpression conditions. In *TAAL* knockdown cells, we observed increased *Tie1* and *Tie2*
304 protein expression. Additionally, there was increased clustering of *Tie1* proteins and enhanced
305 colocalization of *Tie1* and *Tie2* within the cells. Conversely, overexpression of lncRNA *TAAL*

306 significantly reduced the *Tie1* and *Tie2* protein signals and decreased colocalization of *Tie1* and
307 *Tie2* (Figure 5C).
308

309 **LncRNA *TAAL* modulates *Tie1/2* protein turnover by ubiquitination.**

310 To elucidate the mechanisms underlying *Tie1/2* protein turnover, we employed proteomics using
311 LC/MS mass spectrometry on *TAAL* knockdown cells to identify the active pathways involved
312 (Figure 6A). Our gene ontology (GO) molecular function analysis revealed translation
313 dysregulation within cells upon knockdown of the lncRNA *TAAL*. Additionally, we observed the
314 upregulation of proteins with ubiquitin ligase inhibitor and ubiquitin-protein transferase inhibitor
315 activity (Figure 6B-C). To further validate our observation, we conducted a protein stability
316 assay using cycloheximide (10μM) treatment under conditions of both knockdown and
317 overexpression of lncRNA *TAAL*. Cycloheximide-mediated inhibition of translation resulted in
318 decreased stability of the *Tie1* protein in both knockdown and overexpression scenarios. This
319 indicates that the stability of *Tie1* is translation-dependent, with translation inhibition leading to
320 reduced *Tie1* stability (Figure 6D).

321 Previous studies have suggested that *Tie* protein degradation occurs via the proteasomal
322 pathway (Cheng & Hung, 2013; Wehrle *et al*, 2009) and as a receptor kinase, *Tie* may also be
323 degraded through the lysosomal pathway(Gu *et al*, 2022; Zhao *et al*, 2022; Kreitman *et al*, 2018).
324 To investigate this, we inhibited both the lysosomal and proteasomal pathways using the
325 pharmacological drug bafilomycin A1 (50nM) for lysosome and MG132(10μM) for proteasome
326 under conditions of knockdown and overexpression of lncRNA *TAAL*. Lysosomal pathway
327 inhibition enhanced *Tie1* protein stability, whereas proteasomal pathway inhibition compromised

328 stability and increased degradation (Figure 6E). These findings suggest that *Tie1* degradation
329 involves both pathways, with proteasomal inhibition leading to increased lysosomal degradation.
330 Next, we examined the ubiquitination patterns of *Tie1* and *Tie2* proteins as its associated
331 pathways were altered in proteomics studies. Knockdown of lncRNA *TAAL* resulted in increased
332 ubiquitination of *Tie1* and decreased ubiquitination of *Tie2*. Conversely, overexpression of
333 lncRNA *TAAL* led to decreased ubiquitination of *Tie1* and increased ubiquitination of *Tie2*
334 (Figure 6F). These findings and insights from previous literature suggest that lncRNA *TAAL* may
335 mediate the recruitment of specific ubiquitin ligases to *Tie1*, facilitating its ubiquitin-mediated
336 lysosomal degradation. In the absence of lncRNA *TAAL*, the recruitment of appropriate ubiquitin
337 ligases is impaired. Alternatively, we hypothesize that in the absence of *TAAL,* there could be the
338 formation of heterotypic chains of ubiquitin on *Tie1* protein, leading to the binding of other
339 ubiquitin-like proteins and thereby enhancing its stability (Figure 6G). Furthermore, the
340 upregulation of ubiquitin ligase inhibitors under *TAAL* knockdown conditions significantly
341 modulates the ubiquitin-degradation system, which is essential for the targeted degradation of
342 *Tie1* proteins. The stability of both *Tie1* and *Tie2* proteins is enhanced by inhibiting ubiquitin
343 ligases. These observations indicate that lncRNA *TAAL* plays a crucial role in regulating the
344 ubiquitin-mediated lysosomal degradation of *Tie1/2*, thereby controlling protein turnover.
345

346 **lncRNA *TAAL* is negatively regulated in diabetic retinopathy.**

347 To investigate the disease association of lncRNA *TAAL*, we focused on retinopathy, a progressive
348 neovascularization condition often resulting from diabetes. *Tie1/2* signaling pathway has been
349 shown to play an important role in neovascularization during diabetic conditions. Hence we
350 analyzed the expression of lncRNA *TAAL* in endothelial cells under hyperglycemic conditions.

High glucose treatments (25 mM and 50 mM) significantly downregulated lncRNA *TAAL* expression (Figure 7A). Data from the Noncode database revealed that lncRNA *TAAL* is present in extracellular vesicles secreted by HUVEC cells (Figure 7B) (Fang *et al*, 2018). Next, to validate our observation we examined the lncRNA *TAAL* expression in diabetic patients at various stages of retinopathy including patients having diabetes mellitus with no retinopathy (n=50), non-proliferative diabetic retinopathy (NPDR)(n=70), and proliferative diabetic retinopathy (PDR)(n=50) and compared it to control (n=60). We observed a significant enrichment of lncRNA *TAAL* in the blood samples of of NPDR (FC- 2.92; p-value < 0.001) and PDR (FC- 4.107; p-value < 0.001) patients compared to controls and other diabetic conditions (FC- 1.121; p-value - ns) (Figure 7C). Additionally, upon categorizing retinopathy based on its severity we observed that lncRNA TAAL was significantly higher in case of mild NPDR (FC 2.15, *p*-value <0.05), moderate NPDR (FC 3.99, *p*-value <0.001), severe NPDR (FC 2.66, *p*-value <0.05) and PDR (FC 4.1, *p*-value <0.00001) as compared to the healthy controls (Supply Fig 9A-B). Using normalized Ct values from NPDR patients versus controls, ROC curve analysis showed a significant correlation between NPDR and PDR with the lncRNA *TAAL* expression. We also computed the ROC area under the curve and observed a significant specificity and sensitivity for both NPDR (AUC- 0.6763; p-value - 0.004) and PDR (AUC- 0.7649; p-value < 0.0001) compared to control group (Figure 7 D-E). We next modeled the hyperglycemic conditions in HUVEC-hTert2 cells to mimic diabetic retinopathy and to understand the permeability defect associated with this condition. Hyperglycemic condition significantly increased FITC-dextran permeability across the endothelial monolayer (Figure 7F). We also observed decreased surface localization of VE-cadherin, a key adhesion molecule, under hyperglycemic conditions (Figure 7G). Next, we investigated the potential of lncRNA *TAAL* to

modulate endothelial permeability. Overexpression of lncRNA *TAAL* significantly reduced permeability and restored VE-cadherin localization to the membrane under hyperglycemic conditions, as it decrease the *Tie1/2* levels inside the cells..

To investigate the transcriptional regulation and impact of complementation on *TAAL* lncRNA under hyperglycemic conditions, we employed a luciferase reporter assay. This approach allowed us to determine whether the expression of lncRNA *TAAL* is regulated via a positive feedback loop upon complementation in hyperglycemia condition. We cloned the lncRNA *TAAL* promoter into the psiCHECK2 plasmid upstream of Renilla luciferase and performed assays in normal and hyperglycemic conditions. Hyperglycemia significantly decreased luciferase activity, suggesting high glucose inhibits lncRNA *TAAL* transcription. Furthermore, overexpression of lncRNA *TAAL* restored its transcription, indicating a positive feedback loop modulating its own expression. These data collectively underscore the significant role of lncRNA *TAAL* in modulating pathological conditions associated with diabetic retinopathy. We hypothesize that under hyperglycemic conditions, the transcription of lncRNA *TAAL* is downregulated by inhibiting its transcription. This process creates an environment that increases *Tie1* stability and promotes neovascularization, leading to pathological diabetic retinopathy. lncRNA *TAAL* has potential as a biomarker for predicting the progression from normal diabetes to diabetic retinopathy, as it is released into the bloodstream during retinopathy and can be detected by qRT-PCR. Furthermore, lncRNA *TAAL* exhibits high therapeutic potential for restoring normal conditions under hyperglycemia.

Discussion

In this study, we utilized a protein-centric approach to identify interacting partners of the major endothelial receptor protein *Tie1* in HUVEC-hTert2 cells. We identified a novel, uncharacterized

398 lncRNA named *TAAL*, whose modulation influences vascular function and integrity. Further
399 investigations revealed that lncRNA *TAAL* modulates cellular calcium dynamics, affects
400 cytoskeletal movements, and regulates VE-cadherin localization at cell junctions(Figure 3).
401 Molecular analyses provided evidence that lncRNA *TAAL* controls the protein turnover of *Tie1*
402 through the regulation of ubiquitin-mediated degradation and stability. Moreover, we identified a
403 functional orthologue of human lncRNA *TAAL* in zebrafish, which does not exhibit any sequence
404 conservation but has a common interacting partner *Tie1*. Knockdown of zebrafish *taal* resulted
405 in angiogenic defects in the ISVs and SIVs (Figure 4 E-H). Rescue experiments demonstrated
406 that human lncRNA *TAAL* can complement the function of zebrafish lncRNA *taal*, suggesting
407 evolutionary conservation of function (Figure 4F). Our findings propose a negative regulatory
408 role of *TAAL* over *Tie1,* thereby modulating its protein turnover. We further investigated the role
409 of lncRNA *TAAL* in diabetic retinopathy a neovascular eye disease. We observed that the
410 expression of lncRNA *TAAL* was significantly upregulated in patients with NPDR and PDR
411 conditions (Figure 7C). Overexpression of lncRNA *TAAL* in a hyperglycemic model of HUVEC
412 cells decreased permeability defects by restoring VE-cadherin at the membrane (Figure 7F-G).
413 Additionally, overexpression of lncRNA *TAAL* induced a positive feedback loop, which enhanced
414 the transcription of endogenous lncRNA *TAAL* (Figure 7H). Our investigation suggests that
415 lncRNA *TAAL* is an important regulator of *Tie1* protein turnover and could be an effective
416 therapeutic target for neovascular eye diseases.

417 Angiopoietin-Tie signaling is a crucial pathway for targeting various cancers and vascular
418 eye diseases, specifically diabetic retinopathy (Saharinen *et al*, 2017; Joussen *et al*, 2021;
419 Huang *et al*, 2010). *Tie1*, an orphan receptor, has been identified as an interacting receptor for
420 angiopoietin-1 in a heterodimeric form with *Tie2*. In endothelial cells, the dynamics of *Tie1* and
421 *Tie2* interaction and modulation play a significant role in their function. *Tie1* is a major protein
422 associated with the angiogenic function of endothelial cells, particularly when *Tie2* levels are
423 minimal. In the quiescent state, Tie2 levels are upregulated to maintain the survival of

424 endothelial cells, while Tie1 levels remain low. During vascular remodeling, stalk cells exhibit a
425 balance of Tie1 and Tie2 levels, underscoring the importance of both proteins (Savant *et al*,
426 2015). Modulating the interaction and levels of Tie1 and Tie2 *in vivo* holds promise for regulating
427 endothelial cell functions. Inhibition of Angiopoietin-1 has been an effective strategy to modulate
428 Tie1 levels and function during angiogenesis and disease conditions. Additionally, recent
429 findings have identified *LECT2* as a receptor for *Tie1*, showing promising results in controlling
430 angiogenesis and liver fibrosis in vivo (Xu *et al*, 2019). The development of second-generation
431 targeted therapies for *Tie1* using antibodies has also demonstrated encouraging results in
432 preclinical animal models, controlling angiogenesis and metastasis in cancer (Singhal *et al*,
433 2020; La Porta *et al*, 2018). With advancements in RNA modification and the emergence of
434 RNA-based targeted therapies(Sparmann & Vogel, 2023; Saw & Song, 2024; Zhu *et al*, 2022) ,
435 targeting a modulator of *Tie1* protein presents an intriguing approach. Our findings provide
436 evidence that lncRNA *TAAL* can effectively modulate *Tie1* levels *in-vivo,* inhibiting downstream
437 functions to control vascular remodeling. *TAAL* lncRNA serves as a promising candidate for
438 RNA-based target therapy for modulating *Tie1* levels and its associated pathways in vascular
439 diseases such as diabetic retinopathy and cancer metastasis.

440 LncRNAs have been shown to perform myriad functions within cells, primarily
441 determined by their localization to the nucleus, chromatin, or cytoplasm. Cytoplasmic lncRNAs
442 are of particular interest due to their accessibility for therapeutic targeting in various disease
443 conditions. In the cytoplasm, lncRNAs are known to interact with proteins and regulate their
444 functions and translation. Several studies, including those on lncRNAs such as *VEAL2,*
445 *CamK-A, LINK-A, RP11-624L4.1, ECRAR, AGPG, and MetaLnc9 (LINC00963)*, have
446 demonstrated that lncRNAs can interact with kinase proteins and modulate their signaling
447 (Sehgal *et al*, 2021; Sang *et al*, 2018; Lin *et al*, 2016; Zhou *et al*, 2020; Chen *et al*, 2019; Liu *et*
448 *al*, 2020; Yu *et al*, 2017). These interactions suggest roles for lncRNAs in acting as
449 substrate-binding competitors, controlling localization, translation, and stability of kinase

450 proteins. In our investigation, we found that the lncRNA *TAAL* controls the turnover of the
451 receptor kinase *Tie1* protein. We hypothesize that in the absence of *TAAL* lncRNA, *Tie1*
452 undergoes poly-ubiquitination with heterotypic chains of either K6 or K11 linkage, which are
453 known to stabilize the protein (Tracz & Bialek, 2021; Hong *et al*, 2018; Abu Ahmad *et al*, 2021).
454 These K6 and K11 chains of ubiquitin are known to evade lysosomal-mediated degradation by
455 binding with ubiquitin-like proteins, thereby stabilizing the protein. Under normal conditions,
456 poly-ubiquitination with either K63 or K48 linkage homotypic chains is associated with lysosomal
457 degradation (Hong *et al*, 2018). The lncRNA *TAAL* may facilitate proper ubiquitination by
458 recruiting E3 ligase to the *Tie1* protein. In hyperglycemic conditions, there is a complete
459 shutdown of *TAAL* production in endothelial cells, and the remaining *TAAL* is removed via
460 exocytosis. The absence of *TAAL* leads to poly-ubiquitination with heterotypic chains at the *Tie1*
461 kinase domain, where ubiquitin-like proteins attach to these chains and protect them from
462 degradation. Understanding the targets involved in proper ubiquitination of *Tie1* and the
463 ubiquitin-like proteins that protect *Tie1* from degradation warrants further investigations. The
464 protection of *Tie1 from degradation leads* to activation of *Tie1* downstream signaling cascades.
465 This in turn results in change in cytoskeleton dynamics due to dysregulation of calcium
466 dynamics, and alteration in localization of VE-cadherin on the surface of the cells (Figure 8). In
467 this study we provide a detailed assessment and molecular function of lncRNA *TAAL* in vascular
468 remodeling. Going forward, a comprehensive investigation is required to elucidate further the
469 ubiquitination machinery involved in regulating *Tie1* expression.

470 Protein-centric targeted approaches in identifying lncRNA interactomes have shown
471 great promise in selecting lncRNA modulators of disease-associated protein targets. These
472 approaches are valuable not only for identifying orthologous lncRNAs across species that lack
473 sequence conservation but also for understanding the multifaceted roles of lncRNAs in various
474 biological processes(Ranjan *et al*, 2021; Diederichs, 2014; Ulitsky, 2016). Our recent work
475 demonstrated that lncRNA *veal2* which was identified in zebrafish, has shown its interaction with

476 *prkcb2*. A protein-centric pulldown technique was utilized to identify the human ortholog for
477 zebrafish *veal2* without sequence conservation. *VEAL2* was shown to be a promising target and
478 biomarker for proliferative diabetic retinopathy (PDR) patients, regulating vascular permeability
479 (Sehgal *et al*, 2021). Similarly, lncRNA *JPX* a modulator of *XIST* lncRNA, which interacts with
480 the *CTCF* protein, highlighted that this interaction is a conserved function of lncRNA *JPX*
481 despite the absence of sequence conservation between human and mouse ortholog (Karner *et*
482 *al*, 2020). In this study, we observed that despite the lack of sequence conservation between
483 human and zebrafish lncRNA *TAAL*, *Tie1* is a conserved interacting partner, and *TAAL* functions
484 similarly in both species. The conservation of lncRNA functions across species, even in the
485 absence of sequence conservation, underscores the importance of considering alternative
486 modes of conservation. Conservation based on motif or syntenic conservation has only
487 identified a small proportion of orthologues and a large number of lncRNA remains unknown for
488 their mode of conservation. Since many lncRNAs show little to no sequence conservation,
489 focusing on protein-centric interactions can fill critical gaps in our understanding of lncRNA
490 conservation and function. This targeted protein-centric approach can effectively identify
491 functional conserved orthologous lncRNAs, providing insights into their evolutionary significance
492 and biological roles.

493 In summary, we have identified a novel and uncharacterized lncRNA, *TAAL*, using a
494 protein-centric pulldown approach. LncRNA *TAAL* plays a significant role in endothelial cell
495 migration, permeability, and angiogenesis. By using *Tie1* as bait, we also identified the zebrafish
496 ortholog of *TAAL*. Knockdown of zebrafish *taal* resulted in angiogenic defects in the
497 intersegmental vessels (ISV) and subintestinal vessels (SIV), which were successfully rescued
498 by human *TAAL*. Molecular investigations revealed that lncRNA *TAAL* regulates *Tie1* protein
499 turnover by modulating its ubiquitination and subsequent degradation. Additionally, we observed
500 that lncRNA *TAAL* levels were significantly upregulated in patients with diabetic retinopathy
501 (NPDR & PDR), indicating its potential clinical relevance. Overexpression of lncRNA *TAAL* in

502 hyperglycemic conditions restored endothelial cell permeability defects by enhancing the
503 recruitment of VE-cadherin to membrane junctions. Our findings suggest that lncRNA *TAAL*
504 plays a crucial role in regulating *Tie1* stability and function, highlighting its potential as a
505 therapeutic target for vascular eye diseases.

506 **Structured Methods - Reagents and Tools Table**

Reagent/Resource	**Reference or Source**	**Identifier or Catalog Number**
Experimental Models		
gib004Tg(fli1a:EGFP; *gata1a*:DsRed) (*Danio rerio*)	Sridhar Sivasubbu lab, CSIR-IGIB,(Lalwani *et al*, 2012; Lawson & Weinstein, 2002; Traver *et al*, 2003)	*gib004Tg(fli1a*:EGFP; *gata1a*:DsRed)
HUVEC-hTERT2	ATCC	CRL-4053
Recombinant DNA		
pcDNA3.1+	Thermo scientific	V79020
pcDNA-TAAL	This study	Gene script
HA-Ubiqutin plasmid	Addgene	18712
psi-CHEK-2	Promega	C8021
Antibodies		
Tie1	Thermo scientific	PA5-32618
IgG	Abcam	ab231712
Tie2	Cell Signaling Technology	23111S
Tie1	Cell Signaling Technology	4224S
GAPDH	Cell Signaling Technology	2118S
VE-Cadharine	Abcam	ab33168
Alexa Fluor™ 488	Thermo scientific	
Alexa Fluor™ 647	Thermo scientific	
HA antibody	Cell Signaling Technology	3724
Annexin V-FITC	Thermo scientific	A13201
Anti-rabbit IgG, HRP-linked Antibody	Cell Signaling Technology	7074S

Oligonucleotides and other sequence-based reagents		
PCR primers	This Study	Eurofins
taal Morpholino	This study	Gene tools
Scrambled MO	Vivo-Morpholino Standard Control Oligo-Gene tools	Gene tools
Stellaris RNA FISH	This study	LGC Biosearch Technologies
siRNA	Dharmacon	Supply Table
siTAAL	This study	Supply Table
Chemicals, Enzymes and other reagents		
Lipofectamine 3000	Invitrogen	L3000015
Yeast tRNA	Thermo scientific	AM7119
BSA	Sigma	A9418
Vascular Cell Basal Medium	ATCC	PCS-100-030
Endothelial Cell Growth Kit-BBE	ATCC	PCS-100-040
Pierce™ Protein A/G magnetic beads	Thermo Scientific	88803
Proteinase K	HiMedia	
Dual-luciferase reporter assay kit	Promega	E1910
TRIzol	Invitrogen	15596026
N- phenylthiourea	Sigma Aldrich	P7629
T7 mMESSAGE mMACHINE kit	Thermo Scientific	AM1344
3-aminobenzoic acid (Tricaine)	Sigma Aldrich	E10521
TB Green Premix Ex Taq II (Tli RNase H Plus)	Takara	RR82LR
TruSeq RiboPlus RNA Preparation Kit	Illumina	

ProLong™ Gold Antifade Mountant with DNA Stain DAPI	Thermo Scientific	P36941
Corning® Matrigel® Basement Membrane Matrix, *LDEV-Free	Corning	354234
Propidium Iodide	Sigma Aldrich	P4170
Paraformaldehyde	Sigma Aldrich	158127
RNase	Sigma Aldrich	R6148
Fluorescein isothiocyanate–dextran	Sigma Aldrich	46945
Fura-2 AM	Thermo Scientific	F1221
Protease inhibitor cocktail	Roche	04693159001
DyNAmo ColorFlash SYBR Green qPCR Kit	Thermo scientific	F416L
Formaldehyde	Sigma Aldrich	F8775
RIPA lysis buffer	Thermo scientific	89900
Verso cDNA Synthesis Kit	Thermo scientific	AB1453A
SSRT II	Thermo scientific	18064022
Alexa Fluor 488 phalloidin	Thermo scientific	A12379
Sequencing Grade Modified Trypsin	Promega	V5111
Immobilon Forte Western HRP substrate	Sigma Aldrich	WBLUF0500
Software		
Zfin	https://zfin.org/	
STAR v2.7	https://github.com/alexdobin/STAR	
Coding Potential Assessment Tool	http://lilab.research.bcm.edu/	
Coding Potential Calculator	https://cpc.gao-lab.org/	
DESeq2.	https://github.com/thelovelab/DESeq2	

PeakView® software	Sciex	
MarkerView® software	Sciex	
htseq-count	https://github.com/simon-anders/htseq	
GraphPad Prism v9	Graph Pad	
ImageJ FIJI	https://github.com/fiji/fiji	
FlowJo software 10	BD	
Other		
Novaseq 6000	illumina	
Harvard Apparatus pump	Harvard Apparatus	
Stereo microscope Zeiss	ZEISS	
LightCycler LC480	Roche	
CFX384 BioRad	BioRad	
Zeiss Axioscope A1 fluorescent microscope	Carl Zeiss	
Infinite® Lumi plate reader	TECAN	
Zeiense confola mirosoe	Carl Zeiss	
Nikon Eclipse Ti2 microscope	Nikon	
TripleTOF 6600	Thermo scientific	
BD FACSVerse Cell Analyzer	BD	
EVOS	Thermo scientific	

Materials and Method

Ethical approvals

Zebrafish used in this study is a double transgenic zebrafish (*Danio rerio*) *gib004Tg(fli1a*:EGFP; *gata1a*:DsRed) (Lalwani *et al*, 2012; Lawson & Weinstein, 2002; Traver *et al*, 2003). The zebrafish were cared for and maintained in-house following standard operating

513 procedures approved by the Animal Ethics Committee of CSIR-Institute of Genomics and
514 Integrative Biology, India (GENCODE-C-24). Special care was taken to ensure minimal distress
515 to the animals.

516 The human study participants were recruited from Smt. Kannuri Santhamma Centre for
517 vitreoretinal Diseases, L V Prasad Eye Institute, Hyderabad, India. The study was done
518 according to the guidelines of Declaration of Helsinki and study was approved by Institutional
519 Review Board (LEC-BHR-P-04-21-626).

520 **Cell line**

521 We used Human umbilical vein endothelial cell lines HUVEC-hTert2 cell line (CRL-4053,
522 ATCC) for our experiments (Karner *et al*, 2020; Takano *et al*, 2008). The cells were grown in
523 Vascular Cell Basal Medium (PCS-100-030, ATCC) supplemented with Endothelial Cell Growth
524 Kit-BBE (PCS-100-040, ATCC) incubated at 37 C with 5% CO2.

525 **RNA-Immunoprecipitation and RNA-sequencing**

526 For RNA immunoprecipitation, we used ~8 million HUVEC-hTert2 cells from two T75 flasks,
527 and 500 zebrafish embryos at 24 hpf. UV cross-linking was performed according to a previously
528 described protocol. Cell and zebrafish lysates were prepared using RIPA buffer supplemented
529 with protease inhibitors. The cell lysate was incubated with protein A/G beads for pre-clearing
530 for 2 hours at 4°C. Fresh protein A/G beads were blocked using 1x BSA and yeast tRNA for 1
531 hour at room temperature. The cell lysate, protein A/G beads, and the 1ug of primary antibody of
532 *Tie1* (Thermo - PA5-32618) or *Tie2* (CST-23111S) were mixed together and incubated overnight
533 on an orbital rotor at 4°C. The beads were then pulled down and washed with RIPA buffer. The
534 beads were subsequently incubated in PNK buffer with proteinase K at 55°C for 45 minutes.
535 Following incubation, the beads were dissolved in TRIzol, and RNA was isolated using the
536 phenol-chloroform method. The isolated RNA was used for first-strand cDNA preparation using

537 SSRT-II. The RNA-seq library was prepared using the TruSeq RiboPlus RNA Preparation Kit
538 according to the manufacturer's instructions. Finally, the library was sequenced on a NovaSeq
539 6000 platform.
540 The reads were aligned as previously described using STAR aligner to human reference genome
541 hg38 and zebrafish reference genome Zv9 and reads were count using htseq -count function
542 (Dobin *et al*, 2013; Anders *et al*, 2015; Ranjan *et al*, 2024).

543 **Western blot**

544 Cells were lysed using NP40 lysis buffer supplemented with protease inhibitors and quantified
545 using a BCA kit. The lysate was run on a 10% SDS-PAGE gel and transferred to a PVDF
546 membrane. Primary antibodies for *Tie1* (CST-4224S) and *Tie2* (CST-23111S) were diluted to a
547 concentration of 1:1000 and incubated overnight at 4°C. Secondary HRP-conjugated antibodies
548 at 1:10000 dilution were incubated for 1 hour at room temperature. Immunoblotting was
549 visualized using ECL under a chemiluminescence gel documentation system.

550 **Single molecular FISH and Immunofluorescent**

551 We performed smFISH as per the manufacturer's protocol (Biosearch Technologies). Both
552 smFISH and co-immunofluorescence were conducted according to the provided instructions.
553 Briefly, cells were grown on coverslips and fixed in 1% formaldehyde for 10 minutes, followed
554 by three washes with 1X PBS. The cells were then permeabilized using 70% ethanol overnight at
555 4°C. After washing with 1X PBS three times, the cells were incubated in Buffer A for 10
556 minutes. The coverslips were then incubated with a hybridization buffer containing smFISH
557 probes for *TAAL* lncRNA and primary antibody at a 1:200 dilution in a humidified chamber for
558 16 hours at 37°C. Following hybridization, the cells were washed with Wash Buffer A and
559 incubated with a secondary antibody conjugated with Alexa Fluor for 30 minutes in the dark.

560 The cells were subsequently washed with Wash Buffer B, mounted on slides using Anti-fade
561 Gold mounting media with DAPI, and fixed. Confocal imaging of the fixed slides was performed
562 at 63X magnification with oil immersion. The data were processed and deconvolution was
563 performed using FIJI ImageJ software and its plugins (Schindelin *et al*, 2012).

564 **Subcellular fraction**

565 The subcellular fractionation of HUVEC-hTert2 was carried out following a modified version of
566 the protocol described (Ten *et al*, 2012). In brief, T25 flask of HUVEC-hTert2 cells were
567 incubated and homogenized in a hypotonic buffer consisting of 10 mM HEPES (pH 7.9), 1.5
568 mM $MgCl_2$, 10 mM KCl, 0.5 mM DTT, and a protease inhibitor. This mixture was then
569 centrifuged at 1000 rpm for 5 minutes at 4°C. The supernatant, containing the cytoplasmic
570 fraction, was separated, while the pellet, containing the nuclear fraction, was washed with the
571 hypotonic buffer and collected. A small portion (1%) of each sample was set aside for western
572 blot analysis, and the remainder was used for RNA extraction.

573 **Tube formation assay**

574 Tube formation assay was performed on matrigel as previously described (Chatterjee *et al*,
575 2024). Briefly, the knockdown and overexpression of lncRNA TAAL in HUVEC-htert2 cells
576 were taken for the assay. Matrigel was thawed and prepared as per the manufacturer's protocol
577 and was coated in a 48-well plate. 40,000 cells were taken for the assay from each condition and
578 was loaded on top of the solidified matrigel with complete HUVEC mediate. The cells were
579 incubated for 4-5 hrs at 37 °C and 5% CO2 and tube formation was imaged in EVOS or Nikkon
580 microscope.

581 **Scratch wound assay**

582 Scratch wound assay was performed as previously described (Sehgal *et al*, 2021). Briefly,
583 HUVEC-hTert2 cells were transfected with siRNA and pcDNA3.1 plasmid targeting TAAL
584 lncRNA for its knockdown and overexpression. Cells were grown in 24 well plates till the
585 monolayer was formed, and before the experiment, the cells were incubated in HUVEC media
586 without FBS. Using the p200 tip a scratch was made in the well, the media and cell debris were
587 washed using 1 X PBS and incubated in HUVEC media with FBS for 24 hrs, and imaging was
588 done in EVOS or Nikkon microscope.

589 **Annexin -V assay**

590 Cell apoptosis was detected using an Annexin/PI-based assay. The HUVEC-htert2 cells were
591 harvested after transient knockdown and overexpression of TAAL for 48 hours and resuspended
592 in an annexin binding buffer. To this, Annexin V-FITC and Propidium Iodide (PI) were added in
593 the dark for 10 min. Then, the data was acquired using BD FACSVerse Cell Analyzer (BD
594 Bioscience) and the results were analyzed using FlowJo software 10.

595 **Cell cycle assay**

596 To assess cell cycle progression upon knockdown and overexpression of *TAAL*, HUVEC-hTert2
597 cells were seeded in a 6-well plate. After 48 hours, cells were harvested and kept in 70% ethanol
598 for 24 hours at -20 0 C. The next day, cells were treated with RNase at 37 0 C for 1 hour, then
599 stained with Propidium Iodide (PI) in the dark for 30 minutes. The cell cycle distribution was
600 detected using BD FACSVerse Cell Analyzer (BD Bioscience).

601 **Permeability assay**

602 Permeability assay was performed as previously described (Sehgal *et al*, 2021). Briefly, lncRNA
603 TAAL knockdown and overexpressed cells, along with control, were taken for the experiment. 1
604 million cells were seeded on the collagen-coated membrane's upper chamber and incubated until

605 the monolayer is formed. After the monolayer is formed, the media from the upper chamber is
606 removed and supplemented with fresh media with fluorescein isothiocyanate (FITC) conjugated
607 dextran (Sigma, USA) at 1mg/ml final concentration. The sample was incubated and after every
608 30 min, the media from the lower chamber was collected for 3 hours. UV spectrometer reading
609 was taken on a monocular reader, and the FITC-dextrans efflux percentage was calculated.

610 **Ubiquitin assay**

611 The ubiquitin pulldown was performed as previously described (Li *et al*, 2023). Briefly,
612 HUVEC-hTert2 cells were cotransfected with siRNA / overexpression plasmid of TAAL
613 lncRNA with HA-Ubiqutin plasmid (Addgene# 18712). The cells, after 48 hrs of treatment, were
614 treated with MG132 for 8 hours and then harvested. The cells were washed with 1xPBS, and cell
615 lysate was prepared using RIPA buffer (Thermo Scientific) having protease inhibitor and
616 iodoacetamide. Cell lysate was precleared using protein A/G beads, and the primary antibody of
617 target Tie1, and Tie2 was incubated with fresh protein A/G beads separately at room temperature
618 for 2 hr. The cell lysate, proteinA/G bead conjugated primary antibody, was incubated overnight
619 at 4 °C on the orbital rotor. ProteinA/G beads were pulled down and washed 3 times with RIPA
620 buffer. The beads were dissolved in an SDS loading buffer and heated at 95 °C for 10 min. The
621 sample was run on 10% SDS PAGE gel and was transferred on PVDF membrane. The blot was
622 probed with HA antibody at 1:2000 dilution overnight at 4°C and the secondary was incubated at
623 room temperature for 1 hr. Immunoblotting was visualized using ECL under a
624 chemiluminescence gel documentation system.

625 **Morpholino designing and zebrafish microinjection**

626 Antisense morpholino oligonucleotide (MO) was designed to target the exons -intron boundaries
627 of the lncRNA *taal*. The MO was ordered from GeneTools, redissolved in 300 ul to make 1mM

628 stock, and stored in -20 °C for further use. We used 100uM concentration of each MO targeting
629 both the introns and co-injected it into single-cell zebrafish or 2dpf zebrafish at SIV using
630 FemtoJet injection system and Nikkon microscope. After injection, the embryos were transferred
631 to (0.003%) PTU (N- phenylthiourea, Sigma Aldrich) water and further incubated at 28°C. Water
632 was changed every 24 hrs, and dead embryos were discarded. Human lncRNA TAAL was
633 amplified and converted into RNA using Invitro transcription kit T7mMassage mMachine
634 (Thermo scientific). We injected 100ng/ul concentration into single-cell zebrafish or 2dpf
635 zebrafish at SIV as described previously (Habeck *et al*, 2002; Sehgal *et al*, 2021).

636 **RT-qPCR**

637 RNA isolation was done using TRIzol and phenol chloroform method and the samples were
638 DNAses treated. RNA was converted to cDNA using an SSRTII (Thermo scientific) enzyme as
639 instructed by the manufacturer. RT-qPCR was perfomred for taregt gene using TB Green SyBr
640 (Takara) on Biorad CFX96 machine. The data was analyzed as described previously (Winer et
641 al., 1999; Livak and Schmittgen, 2001).

642 **Proteomics**

643 After knockdown using siRNA TAAL and siControl, cells were lysed using RIPA -lysis buffer.
644 Proteins were precipitated with acetone chilled at -20°C. Supernatants were transferred, and four
645 volumes of chilled acetone were added to it. After vortexing and incubation at -20°C for
646 overnight, samples were centrifuged at 10,000 × g for 15 minutes at 4°C. The supernatant was
647 discarded, the pellet air-dried, and resuspended in base buffer (Tris-Cl pH 8 (50 mM)). Protein
648 concentration was determined by BCA assay. This sample was subjected to trypsin digestion
649 (sequencing grade, Promega). 20ug of protein in 20 µl of base buffer was reduced with 2 µl of 25
650 mM DTT at 56°C for 30 minutes, followed by alkylation with 1 µl of 55 mM iodoacetamide at

651 room temperature in the dark for 15 minutes. After adding 2 µl of trypsin (1 µg/µl), samples
652 were incubated at 37°C for 18 hours. Digestion was terminated with 0.5% formic acid, and
653 samples were vacuum evaporated at 30°C.

654 The peptides were fractioned into 8 fractions using a strong cation exchange column- ICAT (AB
655 Sciex). Ellution of the peptide was done with a gradient concentration of ammonium formate
656 buffer. The fractionated peptides were analyzed using a quadrupole-TOF hybrid mass
657 spectrometer (TripleTOF 6600, AB Sciex, USA) coupled with a nano-LC system (Eksigent
658 NanoLC-425) in SWATH mode for relative quantitation. Desalted peptides (5 µg) were initially
659 loaded onto a trap-column (ChromXP C18CL 5 µm 120 Å, Eksigent) for additional desalting.
660 Separation was performed on a reverse-phase C18 analytical column (ChromXP C18, 3 µm 120
661 Å, Eksigent) at a flow rate of 5 µl/minute with buffer A (water containing 0.1% formic acid) and
662 buffer B (acetonitrile containing 0.1% formic acid). Each sample had a runtime of 50 minutes,
663 followed by a 10-minute equilibration period before the next run. The raw data files generated by
664 the instrument were imported into PeakView® software for further analysis. The prepared
665 HUVEC-htert2 proteome ion library was utilized to identify MS/MS peaks, while relative
666 quantitation of different proteins was conducted using MarkerView® software (AB Sciex).

667 **Luciferase assay**

668 The promoter of lncRNA *TAAL* was cloned into the psiCHECK-2 plasmid using *NheI* and *KpnI*
669 restriction enzymes, positioned in front of the renilla luciferase gene. HUVEC-hTert2 cells were
670 transfected with siRNA and an overexpression plasmid for lncRNA *TAAL* along with
671 psiCHEK-2 and psiCHEK-2-TAAL and grown under hyperglycemic (25 mM D-glucose) and
672 normal conditions. Luciferase assays were performed after 48 hrs of transfection according to the
673 manufacturer's protocol (Promega).

674 **Calcium imaging**

675 Calcium imaging was performed as previously described (Arora *et al*, 2021; Motiani *et al*, 2018).
676 Briefly, HUVEC-hTert2 cells, after knockdown and overexpression of lncRNA *TAAL*, were plated
677 on confocal dishes (SPL Life Sciences, Korea). After 48 hours of transfection, the cells were
678 incubated with 4 μM fura-2 AM for 30 minutes at 37°C. The cells were then washed three times
679 with HEPES-buffered saline solution (140 mM NaCl, 1.13 mM MgCl2, 4.7 mM KCl, 2 mM CaCl2,
680 10 mM D-glucose, and 10 mM HEPES; pH 7.4) and bathed for 5 minutes. For calcium imaging,
681 a Nikon Eclipse Ti2 microscope coupled with a CoolLED pE-340 Fura light source and a
682 high-speed PCO camera was used. Excitation was alternated at 340 and 380 nm, and emission
683 was captured at 510 nm. The cells were treated with 10 μM thapsigargin to observe calcium
684 release from the endoplasmic reticulum.

685 **Expression analysis in human blood samples**

686 Blood samples were collected in EDTA-coated vials (for RNA isolation) from individuals with
687 idiopathic macular holes and cataracts as normal controls for this study (n=60). Individuals with
688 diabetic duration of more than 5 and no diabetic retinopathy served as diabetic controls for the
689 study (n=50). Individuals with different forms of DR; mild NPDR (n=20), moderate NPDR
690 (n=25), severe NPDR (n=25) and PDR (n=50) were recruited as cases for this study. Sample
691 demographics are provided in the supply table 2. RNA was isolated from serum. The clot
692 activator vials containing 1 ml blood samples were centrifuged at 1200 rpm for 10 minutes at 4
693 degrees Celsius and the supernatant was collected and stored at -80 degree Celsius until further
694 use. The EDTA coated vials (containing 2 ml blood for RNA isolation) were subjected to series
695 of incubations using the erythrocyte lysis buffer to get rid of red blood cell content and obtain a
696 clear white pellet of white blood cells. RNA was extracted by the organic method using TRIzoL
697 reagent from WBC pellet from blood. Quality and quantity were assessed by agarose gel and

698 nanodrop spectrophotometer respectively. 500 ng of RNA was further reverse-transcribed to
699 cDNA using the Verso cDNA Synthesis Kit (AB1453B). Semi-quantitative PCR was carried out
700 using DyNAmo ColorFlash SYBR Green qPCR Kit (F-416L) and specific primers for lncRNA
701 TAAL. β-actin was used as an endogenous control. Statistical analysis was performed using the
702 student's t-test.
703

704 **Data Availability**

705 All the data has been provided in a supplementary file. Raw sequencing files will be shared upon
706 request.

707 **Conflict of Interest Disclosure**

708 The author declares no conflict of interest

709 **Acknowledgments**

710 This work was funded by DBT/Wellcome Trust India Alliance Fellowship (IA/I/19/2/504651)
711 awarded to Rajender K Motiani. SA acknowledges Senior Research Fellowships from DBT. The
712 authors want to acknowledge Dr. Soumya Sinha Roy and Dr. Barun Chatterjee for their valuable
713 input in cell culture work. We also like to acknowledge Dr. Jyoti Tanwar for assistance and input
714 with calcium imaging and Kriti Khare for assistance with confocal imaging. We also
715 acknowledge the CSIR-IGIB common instrumentation facility, and the ATPC confocal facility,
716 the FACS facility and all the LCSP lab members. Illustrations were made using BioRender.
717

718 **Author's contribution**

719 GR, SSB, RKM conceived and designed the experiment. GR, SA, LS, RB performed the
720 experiments and bioinformatic analysis. SS, SC, IK performed clinical experiments. GR, SSB,

and RKM analyzed the results. GR wrote the initial draft manuscript, and GR, SA, SSB, RKM edited the manuscript.

Reference

Abu Ahmad Y, Oknin-Vaisman A, Bitman-Lotan E & Orian A (2021) From the Evasion of Degradation to Ubiquitin-Dependent Protein Stabilization. *Cells* 10

Anders S, Pyl PT & Huber W (2015) HTSeq--a Python framework to work with high-throughput sequencing data. *Bioinformatics* 31: 166–169

Arora S, Tanwar J, Sharma N, Saurav S & Motiani RK (2021) Orai3 Regulates Pancreatic Cancer Metastasis by Encoding a Functional Store Operated Calcium Entry Channel. *Cancers* 13

Augustin HG, Koh GY, Thurston G & Alitalo K (2009) Control of vascular morphogenesis and homeostasis through the angiopoietin-Tie system. *Nat Rev Mol Cell Biol* 10: 165–177

Bates DO & Curry FE (1997) Vascular endothelial growth factor increases microvascular permeability via a Ca(2+)-dependent pathway. *American Journal of Physiology-Heart and Circulatory Physiology*

Cao X, Li T, Xu B, Ding K, Li W, Shen B, Chu M, Zhu D, Rui L, Shang Z, *et al* (2023) Endothelial TIE1 Restricts Angiogenic Sprouting to Coordinate Vein Assembly in Synergy With Its Homologue TIE2. *Arterioscler Thromb Vasc Biol* 43: e323–e338

Carlantoni C, Allanki S, Kontarakis Z, Rossi A, Piesker J, Günther S & Stainier DYR (2021) Tie1 regulates zebrafish cardiac morphogenesis through Tolloid-like 1 expression. *Dev Biol* 469: 54–67

Chatterjee B, Fatima F, Seth S & Sinha Roy S (2024) Moderate Elevation of Homocysteine Induces Endothelial Dysfunction through Adaptive UPR Activation and Metabolic Rewiring. *Cells* 13

Cheng H-T & Hung W-C (2013) Inhibition of proliferation, sprouting, tube formation and Tie2 signaling of lymphatic endothelial cells by the histone deacetylase inhibitor SAHA. *Oncol Rep* 30: 961–967

Chen Y, Li X, Li B, Wang H, Li M, Huang S, Sun Y, Chen G, Si X, Huang C, *et al* (2019) Long Non-coding RNA ECRAR Triggers Post-natal Myocardial Regeneration by Activating ERK1/2 Signaling. *Mol Ther* 27: 29–45

Dalal PJ, Muller WA & Sullivan DP (2020) Endothelial Cell Calcium Signaling during Barrier Function and Inflammation. *Am J Pathol* 190: 535–542

D'Amico G, Korhonen EA, Waltari M, Saharinen P, Laakkonen P & Alitalo K (2010) Loss of Endothelial Tie1 Receptor Impairs Lymphatic Vessel Development-Brief Report. *Arterioscler Thromb Vasc Biol*

Diederichs S (2014) The four dimensions of noncoding RNA conservation. *Trends Genet* 30:

758 121–123

759 Dobin A, Davis CA, Schlesinger F, Drenkow J, Zaleski C, Jha S, Batut P, Chaisson M &
760 Gingeras TR (2013) STAR: ultrafast universal RNA-seq aligner. *Bioinformatics* 29: 15–21

761 Duh EJ, Sun JK & Stitt AW (2017) Diabetic retinopathy: current understanding, mechanisms,
762 and treatment strategies. *JCI Insight* 2

763 ENCODE Project Consortium, Moore JE, Purcaro MJ, Pratt HE, Epstein CB, Shoresh N, Adrian
764 J, Kawli T, Davis CA, Dobin A, *et al* (2020) Expanded encyclopaedias of DNA elements in
765 the human and mouse genomes. *Nature* 583: 699–710

766 Fang S, Zhang L, Guo J, Niu Y, Wu Y, Li H, Zhao L, Li X, Teng X, Sun X, *et al* (2018)
767 NONCODEV5: a comprehensive annotation database for long non-coding RNAs. *Nucleic*
768 *Acids Res* 46: D308–D314

769 Ferraro NM, Strober BJ, Einson J, Abell NS, Aguet F, Barbeira AN, Brandt M, Bucan M, Castel
770 SE, Davis JR, *et al* (2020) Transcriptomic signatures across human tissues identify
771 functional rare genetic variation. *Science* 369

772 Gavard J (2013) Endothelial permeability and VE-cadherin: a wacky comradeship. *Cell Adh*
773 *Migr* 7: 455–461

774 Gu Y, Becker V, Qiu M, Tang T, Ampofo E, Menger MD & Laschke MW (2022) Brassinin
775 Promotes the Degradation of Tie2 and FGFR1 in Endothelial Cells and Inhibits
776 Triple-Negative Breast Cancer Angiogenesis. *Cancers* 14

777 Habeck H, Odenthal J, Walderich B, Maischein H, Schulte-Merker S & Tübingen 2000 screen
778 consortium (2002) Analysis of a zebrafish VEGF receptor mutant reveals specific
779 disruption of angiogenesis. *Curr Biol* 12: 1405–1412

780 Hamdollah Zadeh MA, Glass CA, Magnussen A, Hancox JC & Bates DO (2008)
781 VEGF-mediated elevated intracellular calcium and angiogenesis in human microvascular
782 endothelial cells in vitro are inhibited by dominant negative TRPC6. *Microcirculation* 15:
783 605–614

784 Hong S-Y, Kao Y-R, Lee T-C & Wu C-W (2018) Upregulation of E3 Ubiquitin Ligase CBLC
785 Enhances EGFR Dysregulation and Signaling in Lung Adenocarcinoma. *Cancer Res* 78:
786 4984–4996

787 Huang H, Bhat A, Woodnutt G & Lappe R (2010) Targeting the ANGPT-TIE2 pathway in
788 malignancy. *Nat Rev Cancer* 10: 575–585

789 Joussen AM, Ricci F, Paris LP, Korn C, Quezada-Ruiz C & Zarbin M (2021) Angiopoietin/Tie2
790 signalling and its role in retinal and choroidal vascular diseases: a review of preclinical data.
791 *Eye* 35: 1305–1316

792 Kang Y-J, Yang D-C, Kong L, Hou M, Meng Y-Q, Wei L & Gao G (2017) CPC2: a fast and

accurate coding potential calculator based on sequence intrinsic features. *Nucleic Acids Res* 45: W12–W16

Karner H, Webb C-H, Carmona S, Liu Y, Lin B, Erhard M, Chan D, Baldi P, Spitale RC & Sun S (2020) Functional Conservation of LncRNA JPX Despite Sequence and Structural Divergence. *J Mol Biol* 432: 283–300

Kreitman M, Noronha A & Yarden Y (2018) Irreversible modifications of receptor tyrosine kinases. *FEBS Lett* 592: 2199–2212

Lalwani MK, Sharma M, Singh AR, Chauhan RK, Patowary A, Singh N, Scaria V & Sivasubbu S (2012) Reverse genetics screen in zebrafish identifies a role of miR-142a-3p in vascular development and integrity. *PLoS One* 7: e52588

La Porta S, Roth L, Singhal M, Mogler C, Spegg C, Schieb B, Qu X, Adams RH, Baldwin HS, Savant S, *et al* (2018) Endothelial Tie1-mediated angiogenesis and vascular abnormalization promote tumor progression and metastasis. *J Clin Invest* 128: 834–845

Lawson ND & Weinstein BM (2002) In vivo imaging of embryonic vascular development using transgenic zebrafish. *Dev Biol* 248: 307–318

Lin A, Li C, Xing Z, Hu Q, Liang K, Han L, Wang C, Hawke DH, Wang S, Zhang Y, *et al* (2016) The LINK-A lncRNA activates normoxic HIF1α signalling in triple-negative breast cancer. *Nat Cell Biol* 18: 213–224

Liu J, Liu Z-X, Wu Q-N, Lu Y-X, Wong C-W, Miao L, Wang Y, Wang Z, Jin Y, He M-M, *et al* (2020) Long noncoding RNA AGPG regulates PFKFB3-mediated tumor glycolytic reprogramming. *Nat Commun* 11: 1507

Li X, Jiang W & Fang M (2023) An optimized protocol to detect ubiquitination modification of exogenous or endogenous proteins. *STAR Protoc* 4: 102650

Motiani RK, Tanwar J, Raja DA, Vashisht A, Khanna S, Sharma S, Srivastava S, Sivasubbu S, Natarajan VT & Gokhale RS (2018) STIM1 activation of adenylyl cyclase 6 connects Ca and cAMP signaling during melanogenesis. *EMBO J* 37

Mueller SB & Kontos CD (2016) Tie1: an orphan receptor provides context for angiopoietin-2/Tie2 signaling. *J Clin Invest* 126: 3188–3191

Pafumi I, Favia A, Gambara G, Papacci F, Ziparo E, Palombi F & Filippini A (2015) Regulation of Angiogenic Functions by Angiopoietins through Calcium-Dependent Signaling Pathways. *Biomed Res Int* 2015: 965271

Papapetropoulos A, Fulton D, Mahboubi K, Kalb RG, O'Connor DS, Li F, Altieri DC & Sessa WC (2000) Angiopoietin-1 inhibits endothelial cell apoptosis via the Akt/survivin pathway. *J Biol Chem* 275: 9102–9105

Pauli A, Valen E, Lin MF, Garber M, Vastenhouw NL, Levin JZ, Fan L, Sandelin A, Rinn JL,

Regev A, *et al* (2012) Systematic identification of long noncoding RNAs expressed during zebrafish embryogenesis. *Genome Res* 22: 577–591

Phoenix KN, Yue Z, Yue L, Cronin CG, Liang BT, Hoeppner LH & Claffey KP (2022) PLCβ2 Promotes VEGF-Induced Vascular Permeability. *Arterioscler Thromb Vasc Biol* 42: 1229–1241

Ranjan G, Scaria V & Sivasubbu S (2024) Syntenic lncRNAs exhibit DNA regulatory functions with sequence evolution. *bioRxiv*

Ranjan G, Sehgal P, Sharma D, Scaria V & Sivasubbu S (2021) Functional long non-coding and circular RNAs in zebrafish. *Brief Funct Genomics*

Reinardy JL, Corey DM, Golzio C, Mueller SB, Katsanis N & Kontos CD (2015) Phosphorylation of Threonine 794 on Tie1 by Rac1/PAK1 Reveals a Novel Angiogenesis Regulatory Pathway. *PLoS One* 10: e0139614

Saharinen P, Eklund L & Alitalo K (2017) Therapeutic targeting of the angiopoietin-TIE pathway. *Nat Rev Drug Discov* 16: 635–661

Saharinen P, Eklund L, Miettinen J, Wirkkala R, Anisimov A, Winderlich M, Nottebaum A, Vestweber D, Deutsch U, Koh GY, *et al* (2008) Angiopoietins assemble distinct Tie2 signalling complexes in endothelial cell-cell and cell-matrix contacts. *Nat Cell Biol* 10: 527–537

Sahu SU, Visetsouk MR, Garde RJ, Hennes L, Kwas C & Gutzman JH (2017) Calcium signals drive cell shape changes during zebrafish midbrain-hindbrain boundary formation. *Mol Biol Cell* 28: 875–882

Sandoval R, Malik AB, Minshall RD, Kouklis P, Ellis CA & Tiruppathi C (2001) Ca(2+) signalling and PKCalpha activate increased endothelial permeability by disassembly of VE-cadherin junctions. *J Physiol* 533: 433–445

Sang L-J, Ju H-Q, Liu G-P, Tian T, Ma G-L, Lu Y-X, Liu Z-X, Pan R-L, Li R-H, Piao H-L, *et al* (2018) LncRNA CamK-A Regulates Ca-Signaling-Mediated Tumor Microenvironment Remodeling. *Mol Cell* 72: 601

Sato TN, Tozawa Y, Deutsch U, Wolburg-Buchholz K, Fujiwara Y, Gendron-Maguire M, Gridley T, Wolburg H, Risau W & Qin Y (1995) Distinct roles of the receptor tyrosine kinases Tie-1 and Tie-2 in blood vessel formation. *Nature* 376: 70–74

Savant S, La Porta S, Budnik A, Busch K, Hu J, Tisch N, Korn C, Valls AF, Benest AV, Terhardt D, *et al* (2015) The Orphan Receptor Tie1 Controls Angiogenesis and Vascular Remodeling by Differentially Regulating Tie2 in Tip and Stalk Cells. *Cell Rep* 12: 1761–1773

Saw PE & Song E (2024) Advancements in clinical RNA therapeutics: Present developments and prospective outlooks. *Cell Rep Med* 5: 101555

Schindelin J, Arganda-Carreras I, Frise E, Kaynig V, Longair M, Pietzsch T, Preibisch S, Rueden C, Saalfeld S, Schmid B, *et al* (2012) Fiji: an open-source platform for biological-image analysis. *Nat Methods* 9: 676–682

Sehgal P, Mathew S, Sivadas A, Ray A, Tanwar J, Vishwakarma S, Ranjan G, Shamsudheen KV, Bhoyar RC, Pateria A, *et al* (2021) LncRNA VEAL2 regulates PRKCB2 to modulate endothelial permeability in diabetic retinopathy. *EMBO J* 40: e107134

Shinde AV, Motiani RK, Zhang X, Abdullaev IF, Adam AP, González-Cobos JC, Zhang W, Matrougui K, Vincent PA & Trebak M (2013) STIM1 controls endothelial barrier function independently of Orai1 and Ca2+ entry. *Sci Signal* 6: ra18

Singhal M, Gengenbacher N, La Porta S, Gehrs S, Shi J, Kamiyama M, Bodenmiller DM, Fischl A, Schieb B, Besemfelder E, *et al* (2020) Preclinical validation of a novel metastasis-inhibiting Tie1 function-blocking antibody. *EMBO Mol Med* 12: e11164

Sparmann A & Vogel J (2023) RNA-based medicine: from molecular mechanisms to therapy. *EMBO J* 42: e114760

Stolz B & Bereiter-Hahn J (1988) Increase of cytosolic calcium results in formation of F-actin aggregates in endothelial cells. *Cell Biol Int Rep* 12: 321–329

Takano H, Murasawa S & Asahara T (2008) Functional and gene expression analysis of hTERT overexpressed endothelial cells. *Biologics* 2: 547–554

Ten S, Hodge K & I. A (2012) Dynamic proteomics: Methodologies and analysis. In *Functional Genomics* InTech

Tiruppathi C, Minshall RD, Paria BC, Vogel SM & Malik AB (2002) Role of Ca2+ signaling in the regulation of endothelial permeability. *Vascul Pharmacol* 39: 173–185

Tracz M & Bialek W (2021) Beyond K48 and K63: non-canonical protein ubiquitination. *Cell Mol Biol Lett* 26: 1

Traver D, Paw BH, Poss KD, Penberthy WT, Lin S & Zon LI (2003) Transplantation and in vivo imaging of multilineage engraftment in zebrafish bloodless mutants. *Nat Immunol* 4: 1238–1246

Tsai F-C & Meyer T (2012) Ca2+ pulses control local cycles of lamellipodia retraction and adhesion along the front of migrating cells. *Curr Biol* 22: 837–842

Tsai F-C, Seki A, Yang HW, Hayer A, Carrasco S, Malmersjö S & Meyer T (2014) A polarized Ca2+, diacylglycerol and STIM1 signalling system regulates directed cell migration. *Nat Cell Biol* 16: 133–144

Ulitsky I (2016) Evolution to the rescue: using comparative genomics to understand long non-coding RNAs. *Nat Rev Genet* 17: 601–614

Wang L, Park HJ, Dasari S, Wang S, Kocher J-P & Li W (2013) CPAT: Coding-Potential Assessment Tool using an alignment-free logistic regression model. *Nucleic Acids Res* 41: e74

Wehrle C, Van Slyke P & Dumont DJ (2009) Angiopoietin-1-induced ubiquitylation of Tie2 by c-Cbl is required for internalization and degradation. *Biochem J* 423: 375–380

Wong TY, Cheung CMG, Larsen M, Sharma S & Simó R (2016) Diabetic retinopathy. *Nature Reviews Disease Primers* 2: 1–17

Xu M, Xu H-H, Lin Y, Sun X, Wang L-J, Fang Z-P, Su X-H, Liang X-J, Hu Y, Liu Z-M, *et al* (2019) LECT2, a Ligand for Tie1, Plays a Crucial Role in Liver Fibrogenesis. *Cell* 178: 1478–1492.e20

Yang H, Luan Y, Liu T, Lee HJ, Fang L, Wang Y, Wang X, Zhang B, Jin Q, Ang KC, *et al* (2020) A map of cis-regulatory elements and 3D genome structures in zebrafish. *Nature* 588: 337–343

Yu T, Zhao Y, Hu Z, Li J, Chu D, Zhang J, Li Z, Chen B, Zhang X, Pan H, *et al* (2017) MetaLnc9 Facilitates Lung Cancer Metastasis via a PGK1-Activated AKT/mTOR Pathway. *Cancer Res* 77: 5782–5794

Zhao L, Zhao J, Zhong K, Tong A & Jia D (2022) Targeted protein degradation: mechanisms, strategies and application. *Signal Transduct Target Ther* 7: 113

Zhou L, Liu R, Liang X, Zhang S, Bi W, Yang M, He Y, Jin J, Li S, Yang X, *et al* (2020) lncRNA RP11-624L4.1 Is Associated with Unfavorable Prognosis and Promotes Proliferation via the CDK4/6-Cyclin D1-Rb-E2F1 Pathway in NPC. *Mol Ther Nucleic Acids* 22: 1025–1039

Zhu Y, Zhu L, Wang X & Jin H (2022) RNA-based therapeutics: an overview and prospectus. *Cell Death Dis* 13: 644

Figure legends

Figure 1: *Tie1-associated angiogenic lncRNA (TAAL)* interaction *Tie1* protein.

[A] Schematic of RNA-immunoprecipitation pipeline for Tie1 protein using HUVEC-hTert2 cell line.

[B] Differential expression analysis of *Tie1/IgG* revealed one enriched lncRNA with a fold change greater than 5, represented in red.

[C] UCSC genome browser snapshot of *TAAL lncRNA* locus in human.

[D] The bar plot represents RNA-immunoprecipitation of *Tie2* in HUVEC-hTert2 cells and shows no enrichment of lncRNA *TAAL.* Data from 3 independent biological replicates plotted as

930 mean fold change ± standard deviation . ns- not significant (two-tailed unpaired t-test)
931 [E] The bar plot depicts the relative abundance of Tie1, Tie2, *TAAL*, GAPDH, β-actin, and
932 MALAT1 in various subcellular fractions quantified using qRT-PCR. *TAAL*, GAPDH, and
933 β-actin show enrichment in the cytoplasmic fraction. Tie1 and Tie2 exhibit equal enrichment in
934 both the cytoplasm and nucleus, while *MALAT1* is predominantly enriched in the nucleus. The
935 data represent relative abundance percentages ± SEM from three independent experiments.
936 [F] Single molecular FISH (smFISH) of *TAAL* (610nM) and Co-IF for Tie1 (GFP) and Tie2
937 (Magenta) highlight their colocalization. Magnification-60x
938
939 **Figure 2: lncRNA *TAAL* modulates pathophysiological function in endothelial cells.**
940 [A-B] Box and whisker plot representing quantification of wound closer rate in scratch wound
941 assay after 24 hrs in control and *TAAL* knockdown or overexpressed cells. *** p-value ≤ 0.001 ;
942 **** p-value ≤ 0.0001. (two-tailed unpaired t-test).
943 [C-D] Bar plot representing quantification of cells migration in the transwell assay compared in
944 control and *TAAL* knockdown or overexpressed cells.* p-value ≤ 0.05; ** p-value ≤ 0.01
945 (two-tailed unpaired t-test).
946 [E-F] Bar plot representing quantification of absorbance in the BrdU proliferation assay
947 compared in control and *TAAL* knockdown or overexpressed cells. ** p-value ≤ 0.01 (two-tailed
948 unpaired t-test).
949 [G-H]Knockdown and overexpression of *TAAL* significantly alter the permeability of
950 dextran-conjugated FITC. Bar plot representing relative dextran-FITC efflux in control and
951 *TAAL* knockdown or overexpressed cells. * p-value ≤ 0.05. (two-tailed unpaired t-test).
952 [I]Knockdown and overexpression of *TAAL* in HUVECs exhibited a reduction in tube formation
953 in Matrigel when compared to the control.
954 [J] Box and whisker plot representing quantification of the number of branched vessels in *TAAL*
955 knockdown (siTAAL) and overexpressed (pcDNA-TAAL) cells along with their controls (
956 siControl; pcDNA3.1). *** p-value ≤ 0.001, **** p-value ≤ 0.0001. (two-tailed unpaired t-test).
957 [K-L] Flow cytometry analysis of cell viability, stained by Annexin V (Q3) and PI (Q1) with
958 viable cells which are negative for both Annexin V and PI (Q4) in control and *TAAL* lncRNA
959 knockdown or overexpression cells.
960

Figure 3: LncRNA *TAAL* modulates cytoskeleton dynamics by altering calcium levels.

[A] Knockdown and overexpression of *TAAL* significantly alter the cytoskeleton dynamics in HUVEC cells. Confocal images of F-actin stained with Alexa Fluor 488 phalloidin in control and *TAAL* knockdown or overexpressed cells (60X magnification). Dot plot representing quantification of aspect ratio (long/short axis) in control and *TAAL* knockdown or overexpressed cells.* p-value ≤ 0.05; ** p-value ≤ 0.01 (two-tailed unpaired t-test).

[B] Representation of Ca^{2+} imaging trace of control and *TAAL* knockdown HUVEC cells with stimulation with thapsigargin (Tg).

[C] Quantification of basal Ca^{2+} levels in control and *TAAL* knockdown HUVEC cells. * p-value ≤ 0.05. (two-tailed unpaired t-test).

[D]Quantification of Ca^{2+} levels release from the endoplasmic reticulum (ER) upon stimulation in Tg in control and *TAAL* knockdown HUVEC cells. *** p-value ≤ 0.001. (two-tailed unpaired t-test).

[E] Representation of Ca^{2+} imaging trace of control and *TAAL* overexpressed HUVEC cells with stimulation with Tg.

[F] Quantification of basal Ca^{2+} levels in control and *TAAL* overexpressed HUVEC cells. ** p-value ≤ 0.01. (two-tailed unpaired t-test).

[G]Quantification of Ca^{2+} levels release from ER upon stimulation in Tg in control and *TAAL* overexpressed HUVEC cells. ** p-value ≤ 0.01. (two-tailed unpaired t-test).

[H] Knockdown and overexpression of *TAAL* significantly alters the localization of VE-Cadhaerin at the junction of HUVEC cells. Confocal images of immunofluorescence VE-Cadhaerin in control and *TAAL* knockdown or overexpressed cells (60X magnification).

Figure 4: Conserved function of lncRNA *TAAL* in zebrafish regulates angiogenesis.

[A] Schematic of RNA-immunoprecipitation pipeline for *tie1* protein using24 hpf zebrfish embryos.

[B] Differential expression analysis of tie1/IgG revealed one enriched lncRNA (ZFLNCG0999) with a fold change greater than 4.5 and $\log_{10}$ P value greater thant 15, represented in red.

[C] Expression pattern of *taal* lncRNA, *tie1* and *tie2* (measured in TPM) across eight distinct developmental stages in zebrafish, utilizing publicly accessible RNA-seq data.

[D] Expression pattern of *taal* lncRNA, *tie1* and *tie2* (measured in TPM) across 12 different

992 tissues using publically available RNA-seq data.

993 [E] Representative images of cranial and trunk vasculature of control and morpholino mediated
994 *taal* knockdown Tg (fli1:eGFP) zebrafish at 24 hpf and 48 hpf at 5x magnification. Bar graph
995 represent quantification of angiogenic defects in control and *taal* knockdown zebrafish. Arrow
996 marks represent the defective angiogenic vessel. **** p-value ≤ 0.0001. (two-tailed unpaired
997 t-test).

998 [F] LncRNA *taal* knockdown enhances angiogesis in zebafish. Representative images of
999 angiogenic sprouting in control and morpholino *taal* injected at at subintestinal vessels (SIVs) in
1000 Tg (fli1:eGFP) zebrafish. Complementation of human lncRNA *TAAL* in morpholino-*taal* injected
1001 Tg(fli1:eGFP) zebrafish at subintestinal vessels (SIVs) halted angiogenic sprouting. Arrow
1002 marks represent the sprouting vessels. Bar graph represent quantification of number of
1003 angiogenic sprotingin in control, *taal* knockdown and *taal* knockdown complimented with
1004 human *TAAL* in zebrafish. ns- not significant; ** p-value ≤ 0.01; *** p-value ≤ 0.001. (two-tailed
1005 unpaired t-test).

1006 [G] Representative images of trunk vasculature of control and *TAAL* overexpression (OE) in Tg
1007 (fli1:eGFP) zebrafish at 48 hpf with 5x magnification. Bar graph represent quantification of
1008 angiogenic defects in control and *TAAL* overexpressed zebrafish. Arrow marks represent the
1009 defective angiogenic vessel. **** p-value ≤ 0.0001. (two-tailed unpaired t-test).

1010 [F] Representative images of angiogenic sprouting in control and Overexpressed *TAAL* injected
1011 at at subintestinal vessels (SIVs) in Tg (fli1:eGFP) zebrafish. Box and whisker plot repent the
1012 area of SIVs in control and Overexpressed *TAAL* injected zebrafish. ** p-value ≤ 0.01
1013 (two-tailed unpaired t-test).

1014

1015 **Figure 5: LncRNA *TAAL* modulates *Tie1* and *Tie2* protein levels.**

1016 [A] Immunoblotting of Tie1 and Tie2 in control and TAAL knockdown or overexpressed cells.
1017 Bar plot representing quantification of blots. * p-value ≤ 0.05; ** p-value ≤ 0.01 (two-tailed
1018 unpaired t-test).

1019 [B] Bar plot representing relative fold change in mRNA expression levels of *Tie1* and *Tie2*
1020 between control and *TAAL* knockdown or overexpressed cells. ns- not significant (two-tailed
1021 unpaired t-test).

1022 [C] Knockdown and overexpression of *TAAL* significantly alters the protein levels of Tie1 and

Tie2 in HUVEC cells. Confocal images of immunofluorescence Tie1 and Tie2 in control and *TAAL* knockdown or overexpressed cells (60X maginication).

Figure 6: LncRNA *TAAL* controls the protein turnover of *Tie1* by modulating it ubiquitination.

[A] Schematic of Protomics quntificatino pipeline for ceontrol and TAAL knockdown cells.

[B] Dot plot representing Gene ontology molecular process for protein downregulated in *TAAL* knockdown cells upon comparing to the control.

[C] Dot plot representing Gene ontology molecular process for protein up-regulated in *TAAL* knockdown cells upon comparing to the control.

[D] Immunobloting of *Tie1* protein upon treatment of cells with translational inhibitor cycloheximide (Chx) for 0, 4, 8 hrs in control and *TAAL* knockdown or overexpressed cells. GAPDH was used as an input control.

[E] Immunobloting of *Tie1* protein upon treatment of cells with degradation inhbitor MG132 and bafilomycin A1(Baf) for 8 hrs in control and *TAAL* knockdown or overexpressed cells. GAPDH was used as an input control.

[F] Change in polyubiqutination of *Tie1* and *Tie2* protein in *TAAL* knockdown or overexpressed cells. Lysates of control and *TAAL* knockdown or overexpressed cells cotrnasfected with HA-Ubiquitin vector were immunoprecipitated with *Tie1* and *Tie2* antibody and immunoblotted with anti-HA antibody.

[G] Hypothetical schematic illustrating the protective effect of lncRNA TAAL on Tie1 through polyubiquitination with heterotypic chains, which attract ubiquitin-like proteins and prevent lysosomal degradation.

Figure 7: LncRNA *TAAL* plays a crucial role in regulating permeability and junctional dynamics in diabetic retinopathy.

[A] Bar graph representing relative fold change levels of TAAL, Tie1, Tie2 upon treatment with hyperglysemia compared to control. ns- not significant; **** p-value $\leq$ 0.0001. (two-tailed unpaired t-test).

[B] Expression profile of *TAAL* lncRNA in exosomes from different cell lines represented in as a bar graph.

[C] Schematics of blood collection and quantification of lncRNA *TAAL* in diabetic and

non-diabetics individuals. Bar graph represents relative fold change expression of lncRNA *TAAL* in blood samples of control, diabetic mellitus (DM), non-poliferative diabetic retinopathy (NPDR) and polyfrerative diabetic retinopathy (PDR) patients.

[D-E] ROC curve analysis determines the sensitivity and specificity of lncRNA *TAAL* as diagnostic biomarker for NPDR or PDR patients with vascular dysfunction.

[F] Complimentation of *TAAL* lncRNA in HUVEC hyperglysemic model reverts the increased permeability. Bar graph represents retalive dextran-FITC efflux in control untreated, control hyperglycemic and *TAAL* overexpressed in hyperglycemic cells. **** p-value ≤ 0.0001. (two-tailed unpaired t-test).

[G] Complimentation of *TAAL* lncRNA in HUVEC hyperglysemic model reverts the localisation of VE-Cadhaerin at the junction of HUVEC cells. Confocal images of immunofluorescence VE-Cadhaerin in control and *TAAL* overexpressed cells under hyperglycemic condition (60X maginication).

[H] Complimentation of *TAAL* lncRNA in HUVEC hyperglysemic model reverts the *in-vivo* expression of *TAAL* by increasing its promoter activity. Luciferase assay of lncRNA *TAAL* promoter in control untreated, control hypoglycemics and *TAAL* overexpressed hyperglycemic cells represented in a bar graph. * p-value ≤ 0.05; ** p-value ≤ 0.01; *** p-value ≤ 0.001 (two-tailed unpaired t-test).

[I] Illustration showing lncRNA TAAL's role in controlling vascular permeability and junctional dynamics through the regulation of Tie1 levels in normal cells. In hyperglycemic conditions, cells downregulate lncRNA TAAL expression and exocytose the residual TAAL transcripts into the bloodstream.

Figure 8: LncRNA *TAAL* controls the protein turnover of *Tie1* and modulates vascular permeability and angiogenic function.

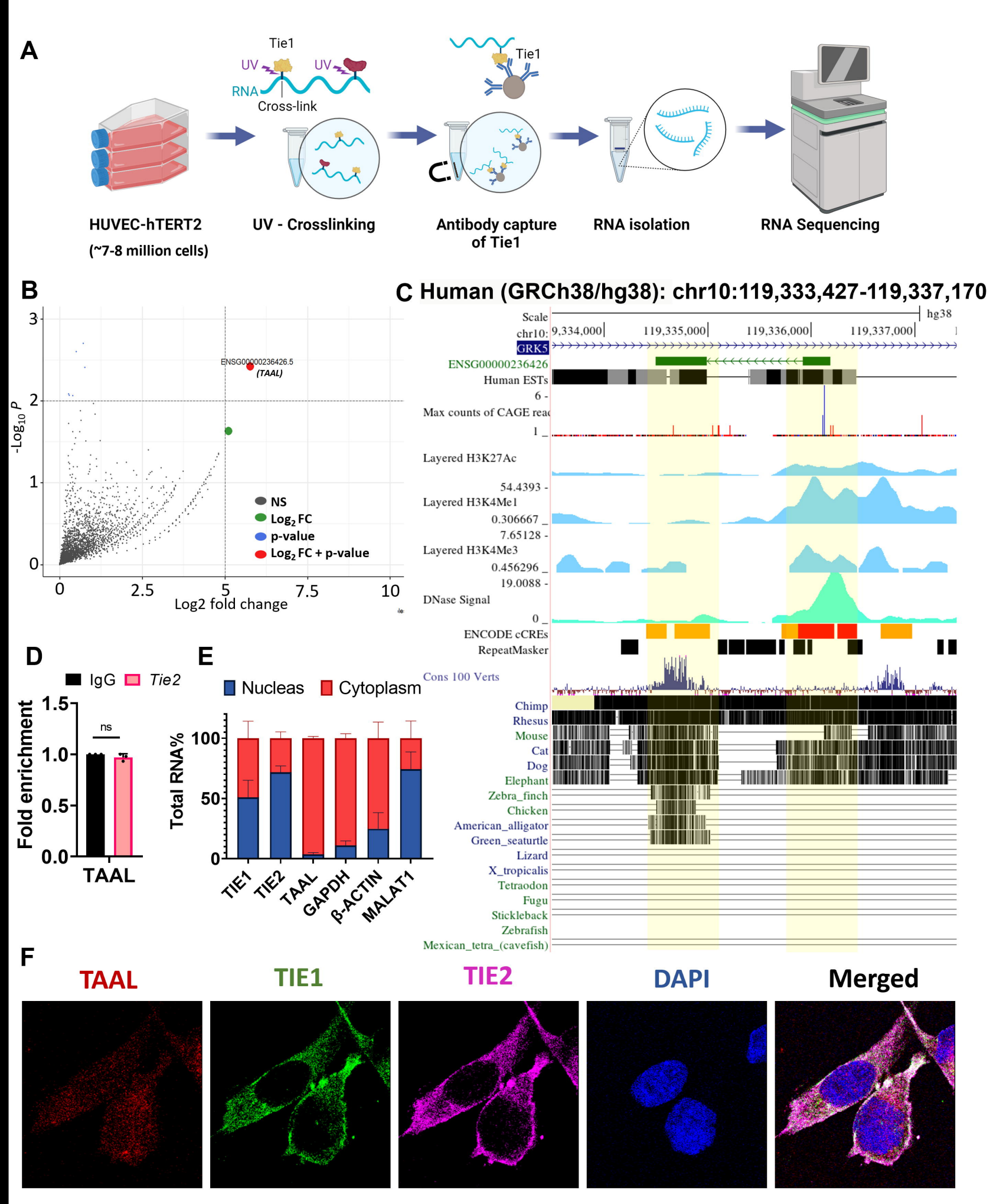
A
Tie1
UV
UV
RNA
Cross-link
Tie1
HUVEC-hTERT2
(~7-8 million cells)
UV - Crosslinking
Antibody capture of Tie1
RNA isolation
RNA Sequencing
B
ENSG00000236426.5
(TAAL)
-Log10 P
Log2 fold change
NS
Log2 FC
p-value
Log2 FC + p-value
C Human (GRCh38/hg38): chr10:119,333,427-119,337,170
Scale
chr10:
hg38
9,334,000
119,335,000
119,336,000
119,337,000
GRK5
ENSG00000236426
Human ESTs
Max counts of CAGE reads
Layered H3K27Ac
Layered H3K4Me1
Layered H3K4Me3
DNase Signal
ENCODE cCREs
RepeatMasker
Cons 100 Verts
Chimp
Rhesus
Mouse
Cat
Dog
Elephant
Zebra_finch
Chicken
American_alligator
Green_seaturtle
Lizard
X_tropicalis
Tetraodon
Fugu
Stickleback
Zebrafish
Mexican_tetra_(cavefish)
D
IgG
Tie2
Fold enrichment
ns
TAAL
E
Nucleas
Cytoplasm
Total RNA%
TIE1
TIE2
TAAL
GAPDH
β-ACTIN
MALAT1
F
TAAL
TIE1
TIE2
DAPI
Merged

Scratch wound assay

Transwell migration assay

A

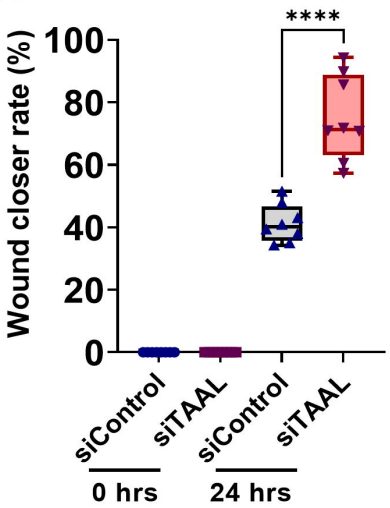

B

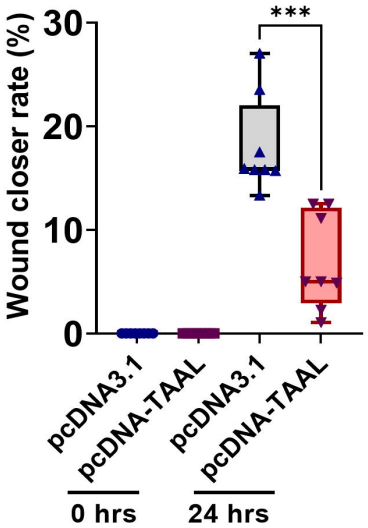

C

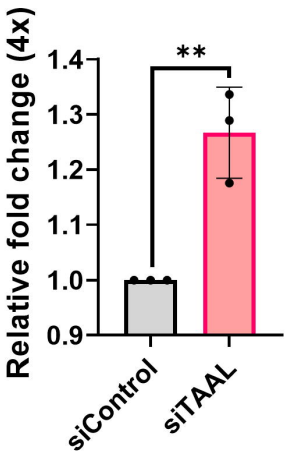

D

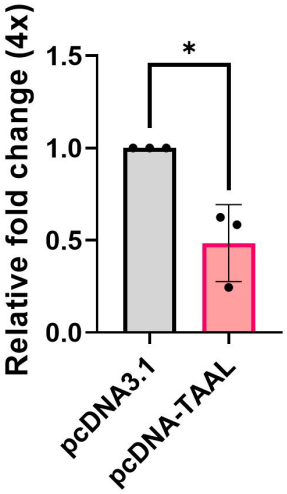

Permeability assay

E

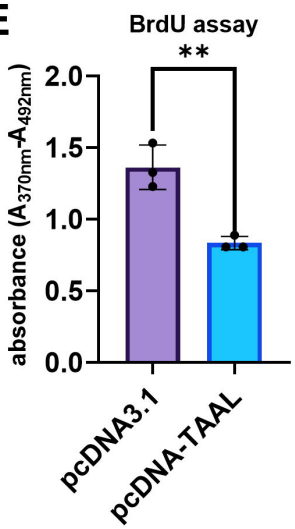

F

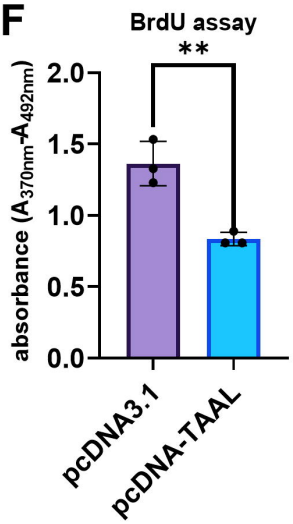

G

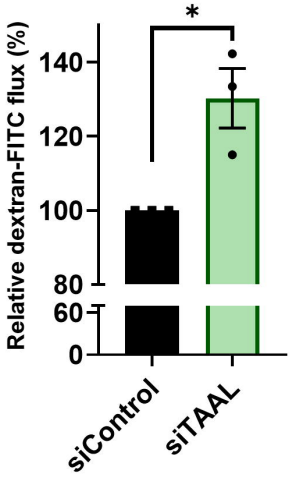

H

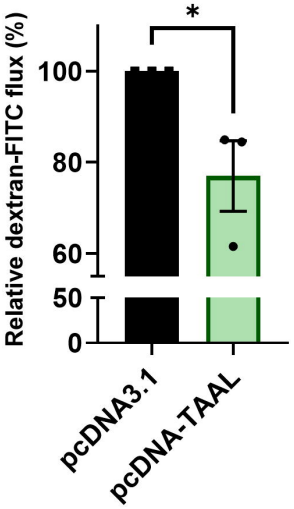

I

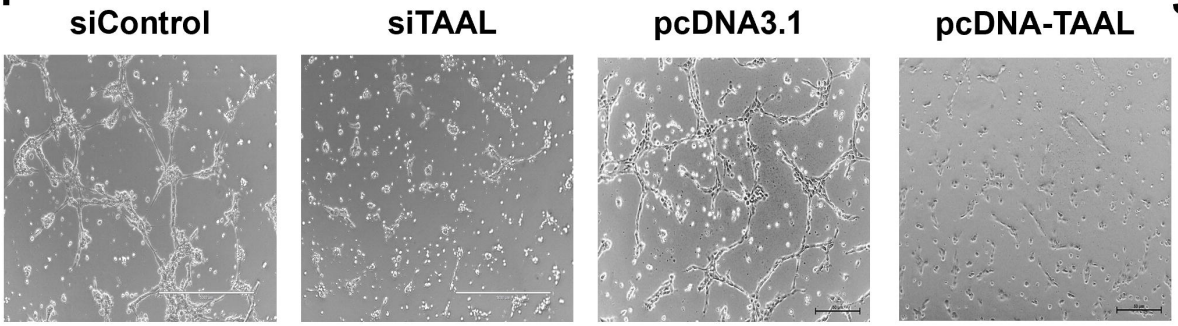

J

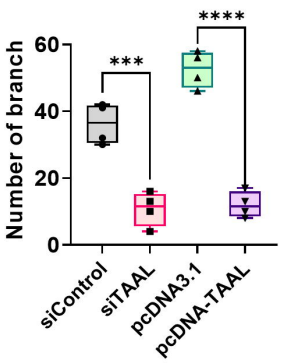

K

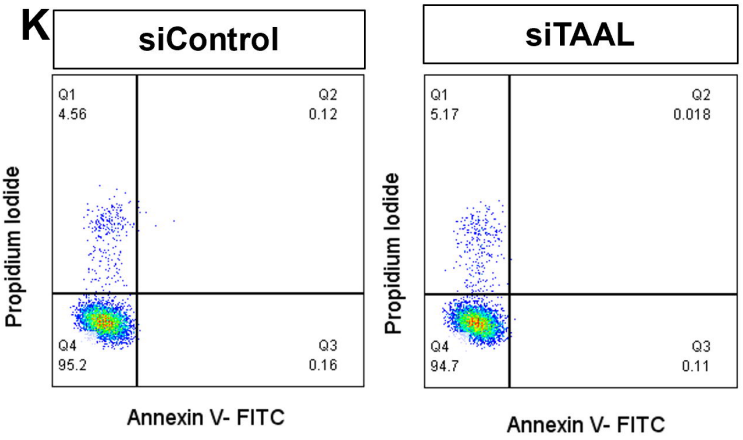

L

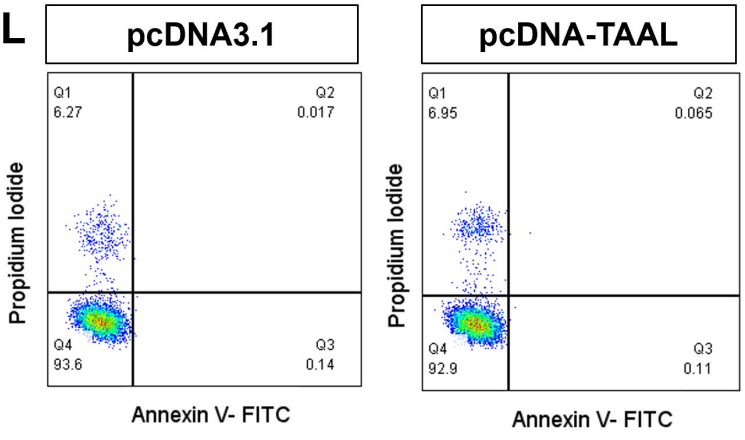

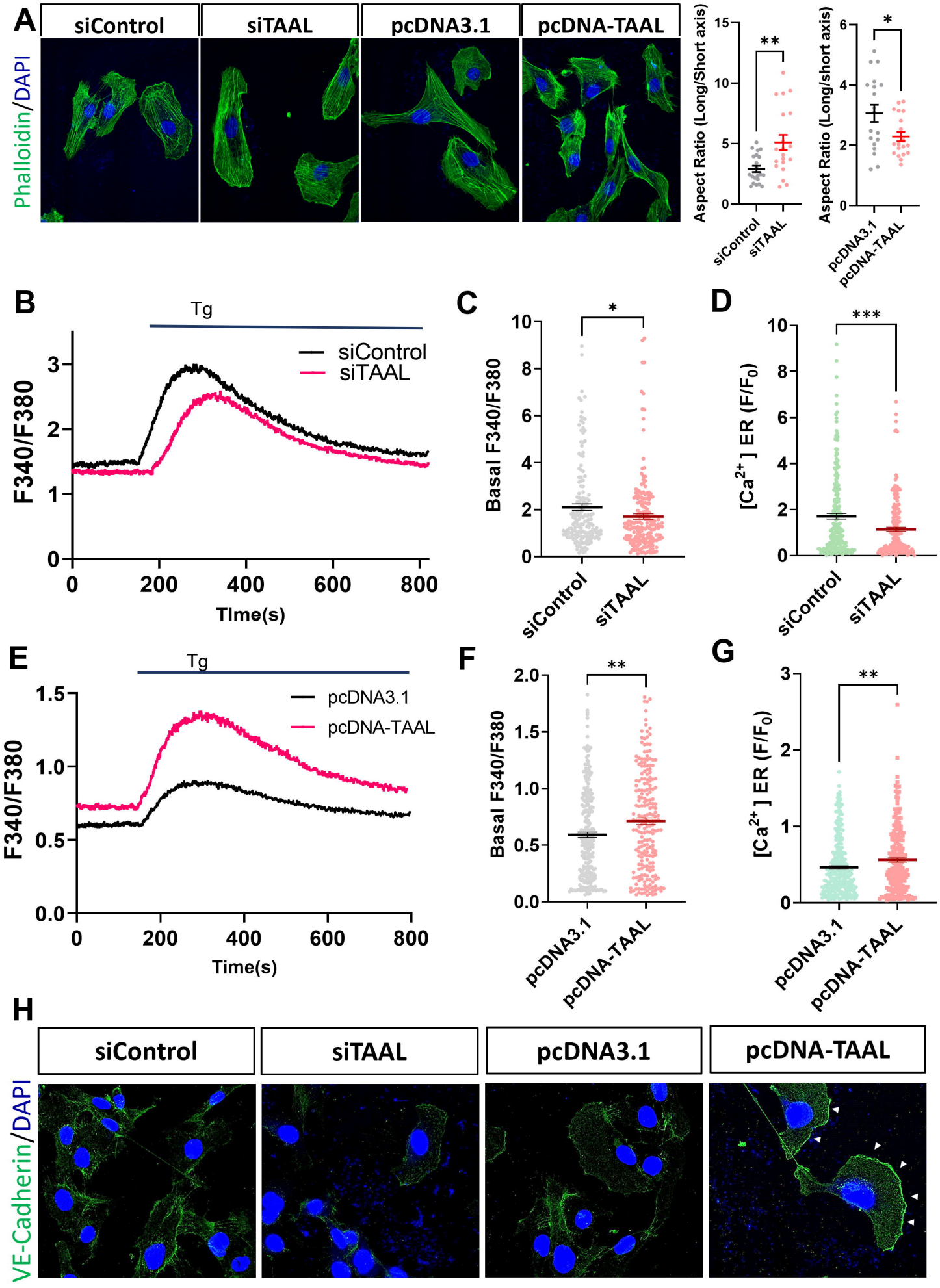
A
siControl
siTAAL
pcDNA3.1
pcDNA-TAAL
Phalloidin/DAPI
Aspect Ratio (Long/Short axis)
**
*
siControl
siTAAL
pcDNA3.1
pcDNA-TAAL
B
Tg
siControl
siTAAL
F340/F380
Time(s)
C
Basal F340/F380
*
D
[Ca2+] ER (F/F0)
***
E
Tg
pcDNA3.1
pcDNA-TAAL
F340/F380
Time(s)
F
Basal F340/F380
**
G
[Ca2+] ER (F/F0)
**
H
siControl
siTAAL
pcDNA3.1
pcDNA-TAAL
VE-Cadherin/DAPI

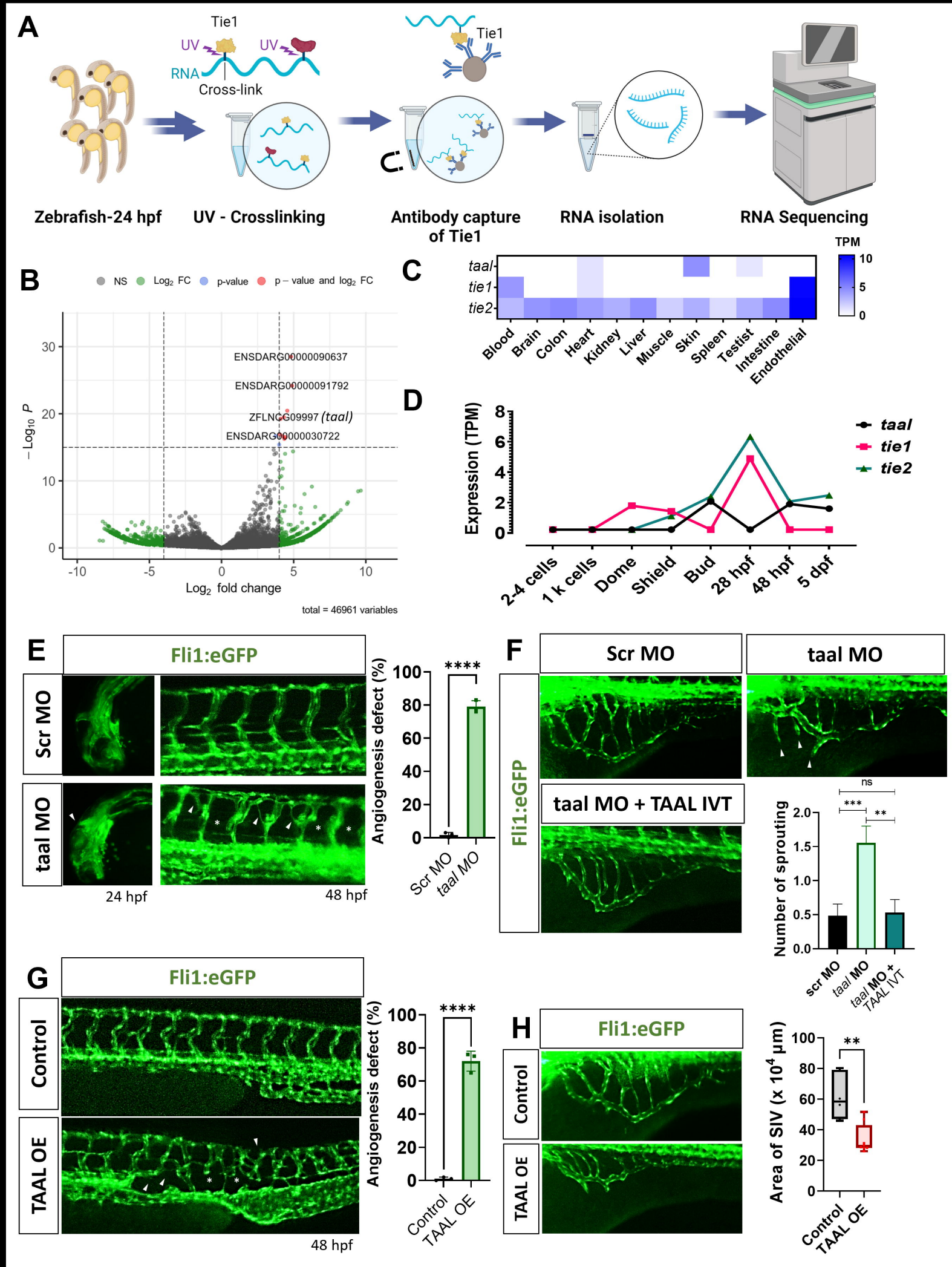
A
Tie1
UV
UV
RNA
Cross-link
Tie1
Zebrafish-24 hpf
UV - Crosslinking
Antibody capture of Tie1
RNA isolation
RNA Sequencing
B
NS
Log2 FC
p-value
p – value and log2 FC
ENSDARG00000090637
ENSDARG00000091792
ZFLNCG09997 (taal)
ENSDARG00000030722
– Log10 P
Log2 fold change
total = 46961 variables
C
TPM
taal
tie1
tie2
Blood
Brain
Colon
Heart
Kidney
Liver
Muscle
Skin
Spleen
Testist
Intestine
Endothelial
D
Expression (TPM)
taal
tie1
tie2
2-4 cells
1 k cells
Dome
Shield
Bud
28 hpf
48 hpf
5 dpf
E
Fli1:eGFP
Scr MO
taal MO
24 hpf
48 hpf
Angiogenesis defect (%)
****
Scr MO
taal MO
F
Scr MO
taal MO
Fli1:eGFP
taal MO + TAAL IVT
Number of sprouting
ns
***
**
scr MO
taal MO
taal MO + TAAL IVT
G
Fli1:eGFP
Control
TAAL OE
48 hpf
Angiogenesis defect (%)
****
Control
TAAL OE
H
Fli1:eGFP
Control
TAAL OE
Area of SIV (x 10^4 µm)
**
Control
TAAL OE

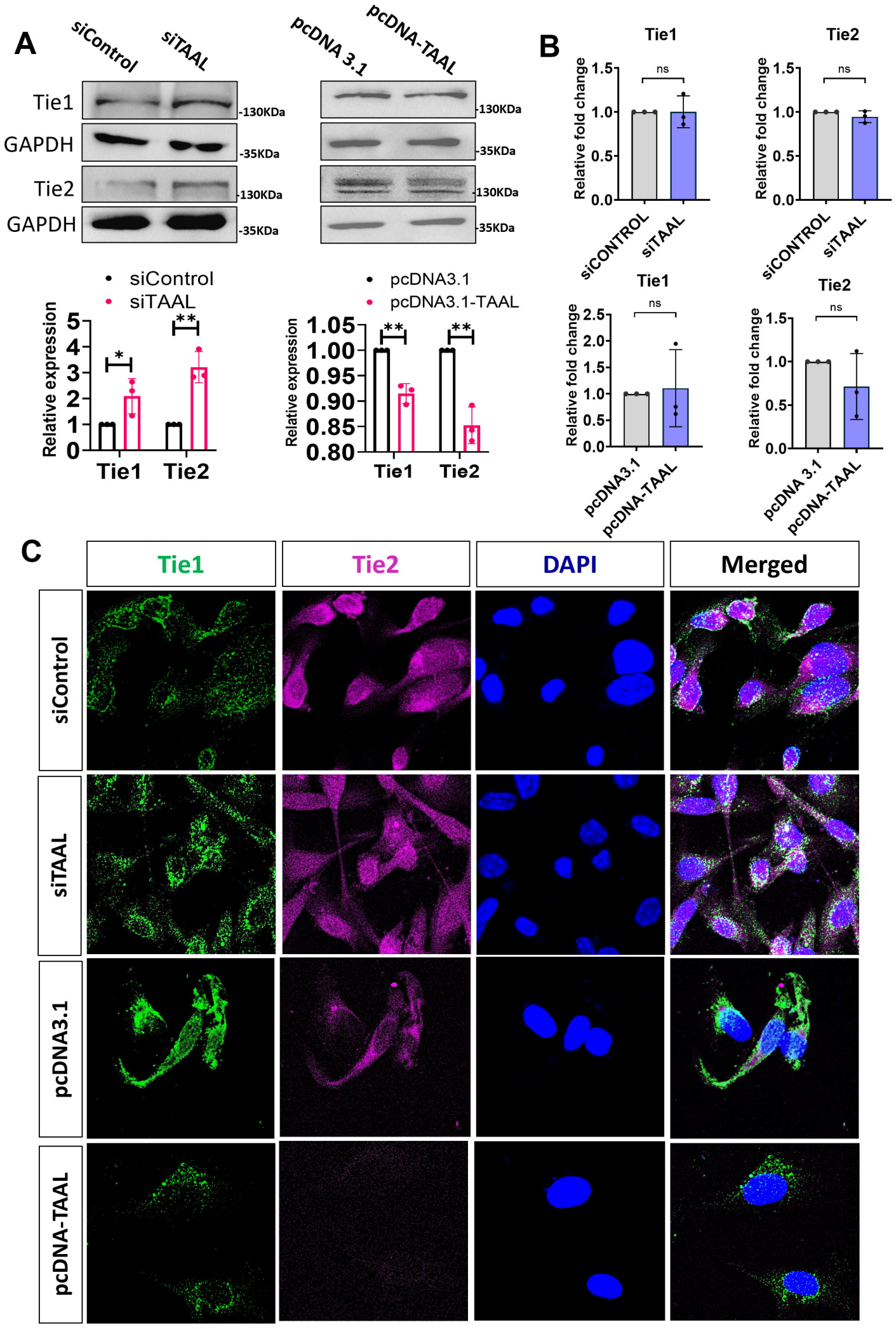
A
siControl
siTAAL
pcDNA 3.1
pcDNA-TAAL
Tie1
GAPDH
Tie2
GAPDH
130KDa
35KDa
siControl
siTAAL
Relative expression
Tie1
Tie2
pcDNA3.1
pcDNA3.1-TAAL
B
Tie1
Tie2
Relative fold change
ns
siCONTROL
siTAAL
pcDNA3.1
pcDNA-TAAL
C
Tie1
Tie2
DAPI
Merged
siControl
siTAAL
pcDNA3.1
pcDNA-TAAL

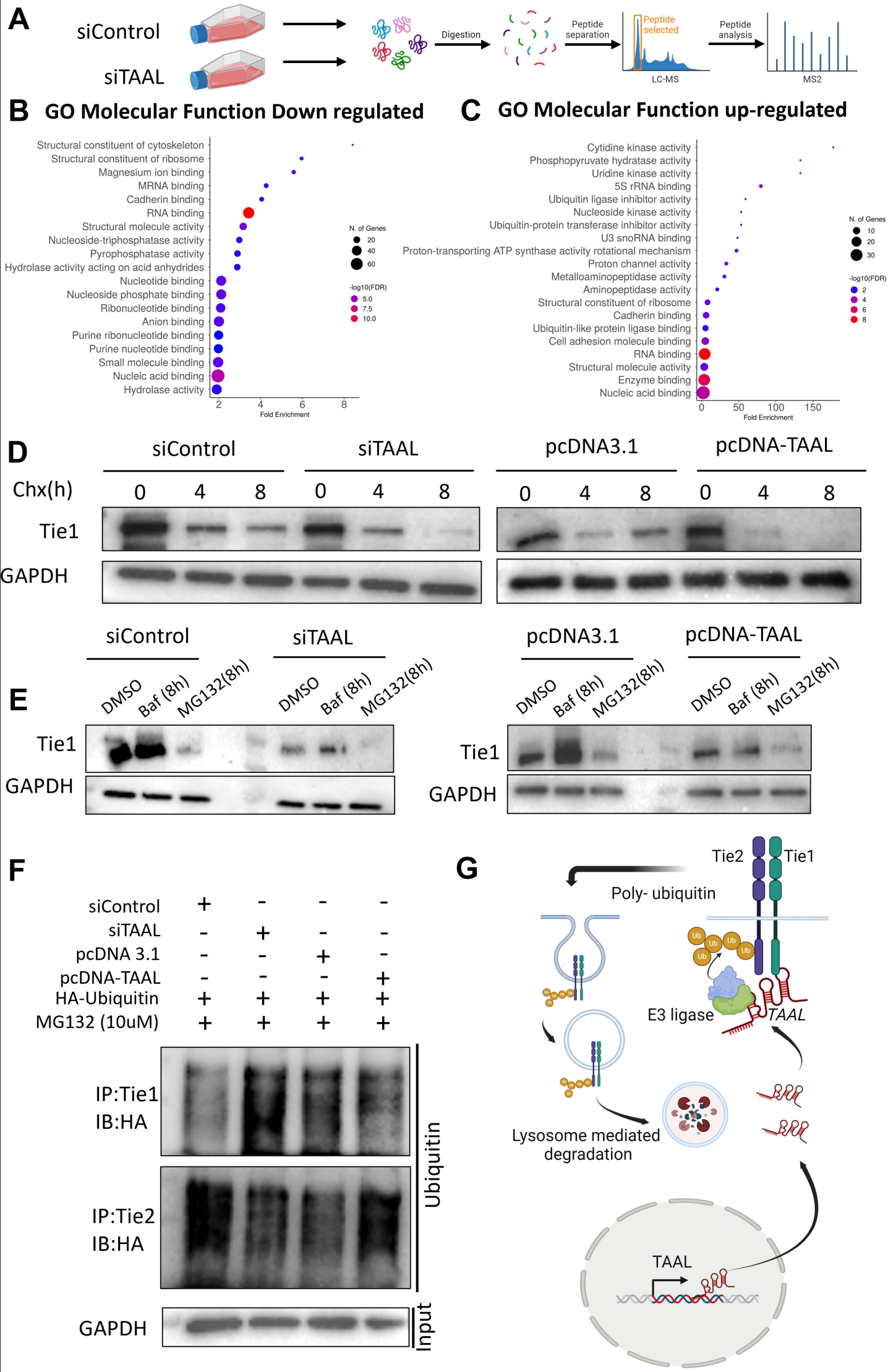
A
siControl
siTAAL
Digestion
Peptide separation
Peptide selected
LC-MS
Peptide analysis
MS2
B GO Molecular Function Down regulated
Structural constituent of cytoskeleton
Structural constituent of ribosome
Magnesium ion binding
MRNA binding
Cadherin binding
RNA binding
Structural molecule activity
Nucleoside-triphosphatase activity
Pyrophosphatase activity
Hydrolase activity acting on acid anhydrides
Nucleotide binding
Nucleoside phosphate binding
Ribonucleotide binding
Anion binding
Purine ribonucleotide binding
Purine nucleotide binding
Small molecule binding
Nucleic acid binding
Hydrolase activity
Fold Enrichment
N. of Genes
-log10(FDR)
C GO Molecular Function up-regulated
Cytidine kinase activity
Phosphopyruvate hydratase activity
Uridine kinase activity
5S rRNA binding
Ubiquitin ligase inhibitor activity
Nucleoside kinase activity
Ubiquitin-protein transferase inhibitor activity
U3 snoRNA binding
Proton-transporting ATP synthase activity rotational mechanism
Proton channel activity
Metalloaminopeptidase activity
Aminopeptidase activity
Structural constituent of ribosome
Cadherin binding
Ubiquitin-like protein ligase binding
Cell adhesion molecule binding
RNA binding
Structural molecule activity
Enzyme binding
Nucleic acid binding
Fold Enrichment
N. of Genes
-log10(FDR)
D
siControl
siTAAL
pcDNA3.1
pcDNA-TAAL
Chx(h)
0 4 8 0 4 8 0 4 8 0 4 8
Tie1
GAPDH
E
siControl
siTAAL
pcDNA3.1
pcDNA-TAAL
DMSO
Baf (8h)
MG132(8h)
Tie1
GAPDH
F
siControl + - - -
siTAAL - + - -
pcDNA 3.1 - - + -
pcDNA-TAAL - - - +
HA-Ubiquitin + + + +
MG132 (10uM) + + + +
IP:Tie1
IB:HA
IP:Tie2
IB:HA
Ubiquitin
GAPDH
Input
G
Tie2
Tie1
Poly- ubiquitin
Ub
E3 ligase
TAAL
Lysosome mediated degradation
TAAL

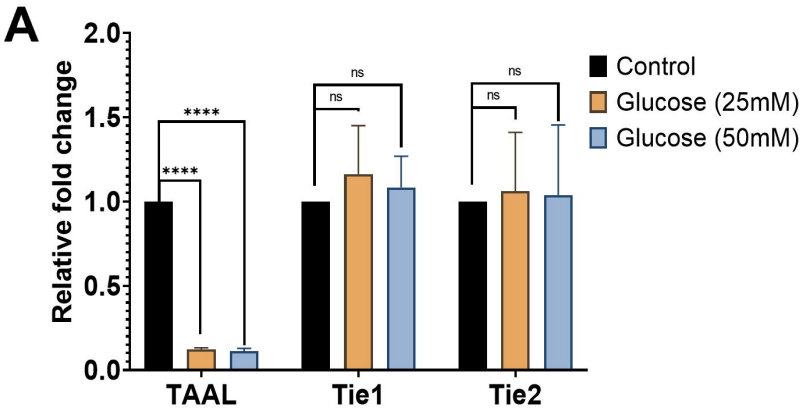
A
Relative fold change
2.0
1.5
1.0
0.5
0.0
****
****
ns
ns
ns
ns
Control
Glucose (25mM)
Glucose (50mM)
TAAL
Tie1
Tie2

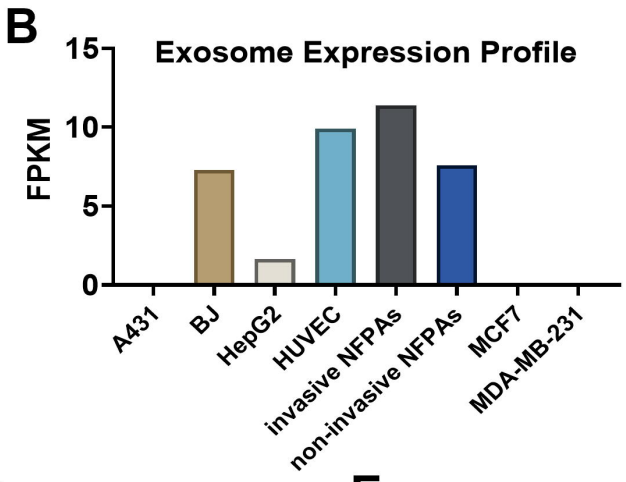
B
Exosome Expression Profile
FPKM
15
10
5
0
A431
BJ
HepG2
HUVEC
invasive NFPAs
non-invasive NFPAs
MCF7
MDA-MB-231

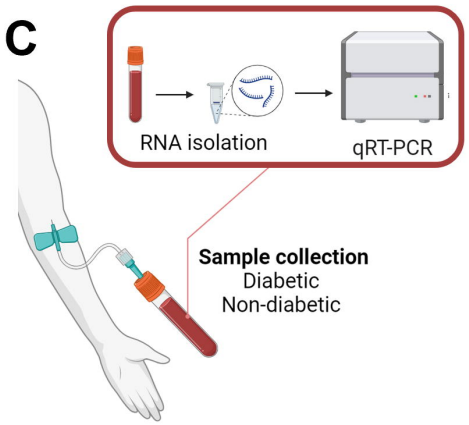
C
RNA isolation
qRT-PCR
Sample collection
Diabetic
Non-diabetic

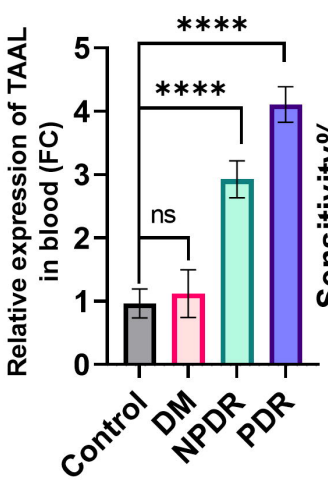
Relative expression of TAAL in blood (FC)
5
4
3
2
1
0
****
****
ns
Control
DM
NPDR
PDR

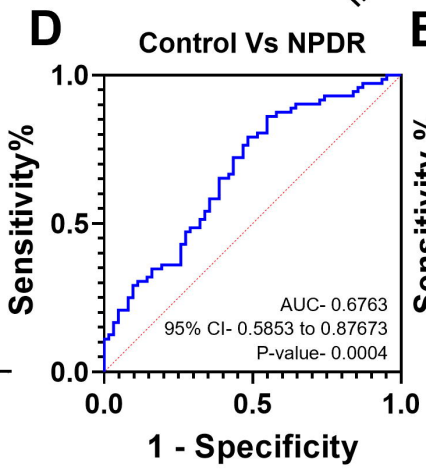
D
Control Vs NPDR
Sensitivity%
1.0
0.5
0.0
AUC- 0.6763
95% CI- 0.5853 to 0.87673
P-value- 0.0004
0.0
0.5
1.0
1 - Specificity

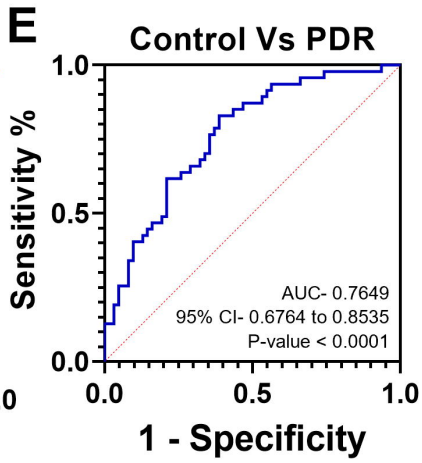
E
Control Vs PDR
Sensitivity %
1.0
0.5
0.0
AUC- 0.7649
95% CI- 0.6764 to 0.8535
P-value < 0.0001
0.0
0.5
1.0
1 - Specificity

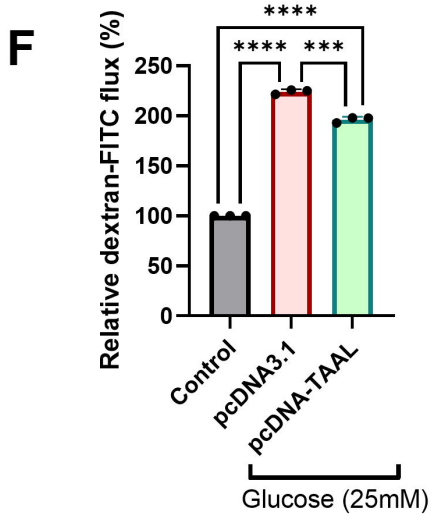
F
Relative dextran-FITC flux (%)
250
200
150
100
50
0
****
****
***
Control
pcDNA3.1
pcDNA-TAAL
Glucose (25mM)

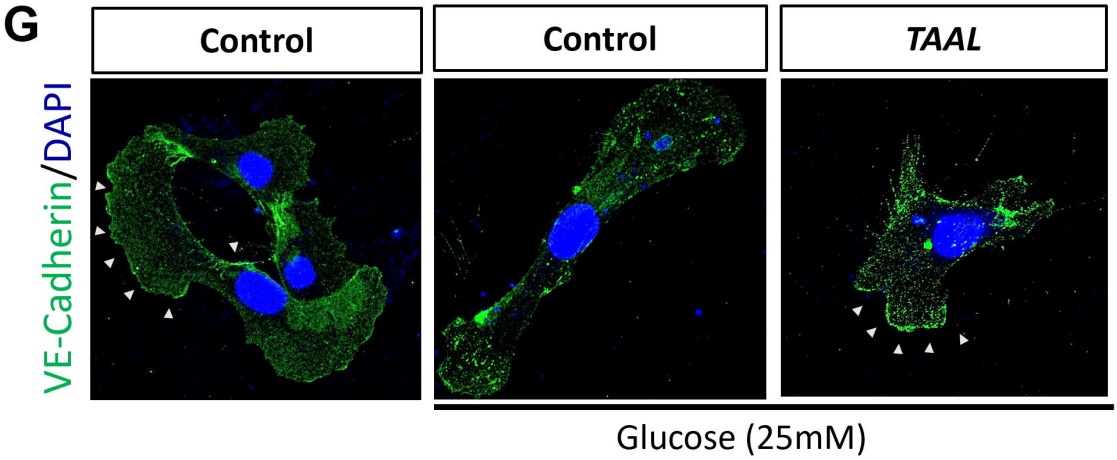
G
Control
Control
TAAL
VE-Cadherin/DAPI
Glucose (25mM)

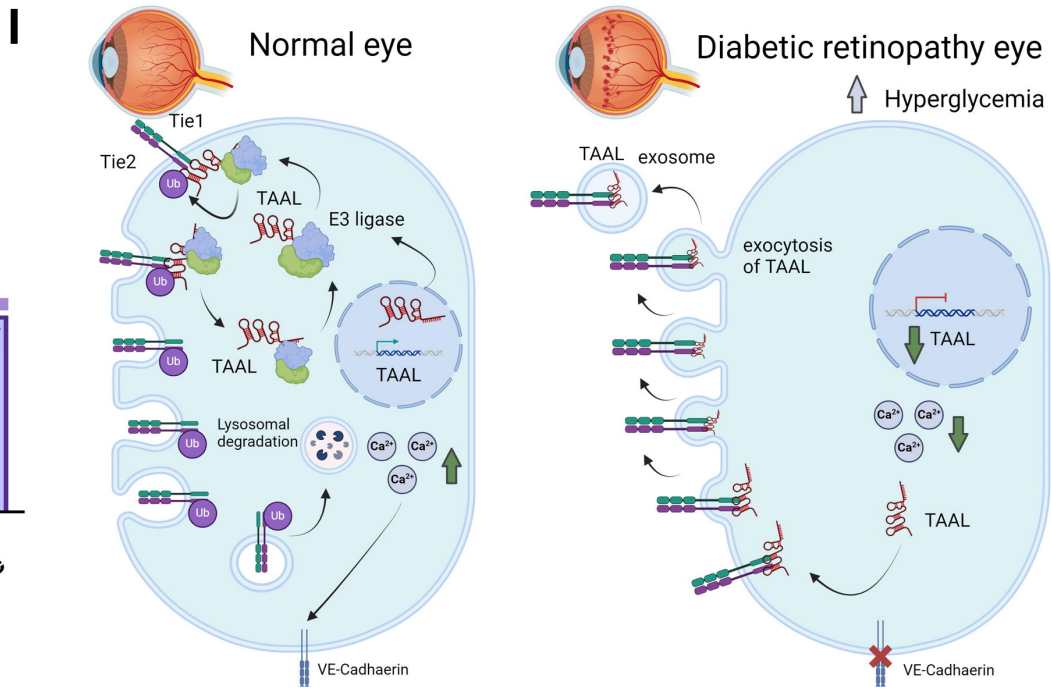
I
Normal eye
Tie1
Tie2
Ub
TAAL
E3 ligase
TAAL
TAAL
Lysosomal degradation
Ca2+
VE-Cadhaerin
Diabetic retinopathy eye
Hyperglycemia
TAAL
exosome
exocytosis of TAAL
TAAL
TAAL
VE-Cadhaerin

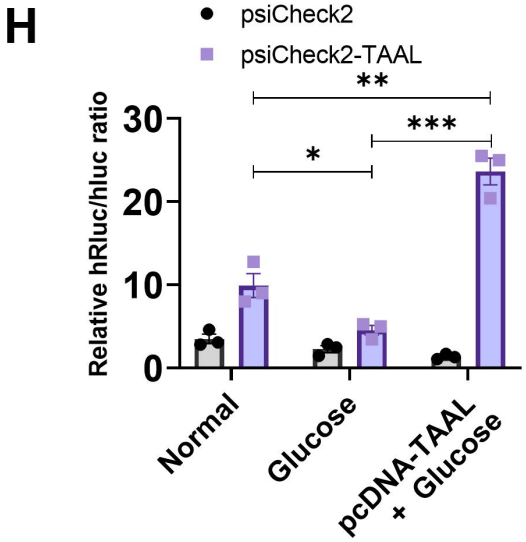
H
psiCheck2
psiCheck2-TAAL
Relative hRluc/hluc ratio
30
20
10
0
**
***
*
Normal
Glucose
pcDNA-TAAL + Glucose

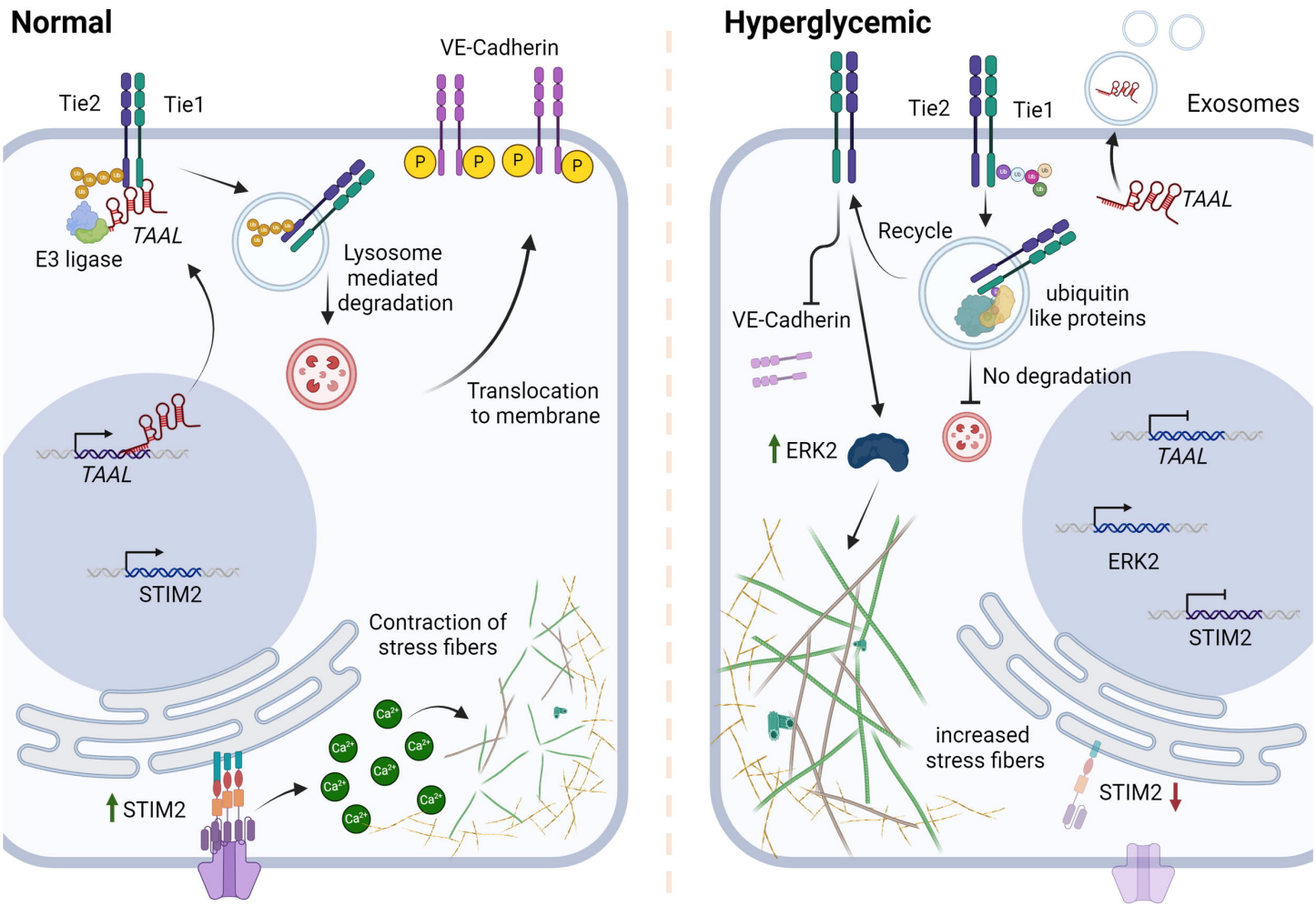
Normal
VE-Cadherin
Tie2
Tie1
P
P
P
P
TAAL
E3 ligase
Lysosome
mediated
degradation
Translocation
to membrane
TAAL
STIM2
Contraction of
stress fibers
Ca2+
STIM2
Hyperglycemic
Tie2
Tie1
Exosomes
TAAL
Recycle
ubiquitin
like proteins
VE-Cadherin
No degradation
ERK2
TAAL
ERK2
STIM2
increased
stress fibers
STIM2